Optical Coherence Tomography for Non-Invasive *ex vivo* Investigations in Dental Medicine — a Joint Group Experience (Review)

Ⓒ

Silvana Canjau, DMD, Associate Professor, Department of Oral Rehabilitation and Dental Emergencies, Faculty of Dentistry[1];
Carmen Todea, DMD, PhD, Professor, Head of the Department of Oral Rehabilitation and Dental Emergencies, Faculty of Dentistry[1];
Meda Lavinia Negrutiu, DMD, PhD, Professor, Department of Dental Materials and Dental Technology, Vice-dean of the Faculty of Dentistry[1];
Cosmin Sinescu, DMD, PhD, Lecturer, Department of Dental Materials and Dental Technology, Faculty of Dentistry[1];
Florin Ionel Topala, DMD, Assistant Professor, Department of Prosthodontics, Faculty of Dentistry[1];
Corina Marcauteanu, DMD, PhD, Lecturer, Head of the Department of Occlusology, Faculty of Dentistry[1];
Adrian Manescu, PhD, Post-Doc, Department of Odontostomatologic and Specialized Clinical Sciences (Di.S.C.O.), Section of Physical Sciences[2];
Virgil-Florin Duma, Engineer, MSc, PhD, Post-Doc, Professor, Head and Founder of the 3OM Optomechatronics Group[3];
Adrian Bradu, Physicist, MSc, PhD, Post-Doc, Research Assistant, Applied Optics Group[4];
Adrian Gh. Podoleanu, Physicist, PhD, Professor, Head of Applied Optics Group[4]

[1]"Victor Babes" University of Medicine and Pharmacy Timisoara, 2 Eftimie Murgu Square, Timisoara, 300041, Romania;
[2]Universita Politecnica delle Marche, 22 Piazza Roma, Ancona, 60100, Italy;
[3]School of Engineering, "Aurel Vlaicu" University of Arad, 77 Revolutiei Avenue, Arad, 310130, Romania;
[4]School of Physical Sciences, University of Kent, Canterbury, Ingram Building, Room 301, CT2 7NH, United Kingdom

This review emphasizes the current knowledge related to optical coherence tomography (OCT) as a non-invasive diagnostic tool to perform *ex vivo* and showing great potential for *in vivo* structural imaging of features in the oral cavity. OCT technology can generate high-resolution cross-sectional and *en-face* images of the internal architecture of the investigated sample (2–3 mm in depth). To this goal, *en-face* time domain OCT (TD-OCT) and spectral domain OCT (SD-OCT) were employed. Topics included in this review refer to OCT non-destructive evaluations of: dental abfraction and attrition, material defects and micro-leakages at the tooth-filling interface, temporal-mandibular joint disc, quality of bracket bonding on dental hard tissue, prosthetic restorations and micro-leakages at prosthetic interfaces, root canals, presence or absence of apical micro-leakages, and osteo-integration of dental implants and of bone grafting materials. OCT revealed internal features of the material investigated with greater sensitivity than current diagnostic methods. We put our research in context with others' results but the review reflects primarily our joint group experience and it presents images collected with our OCT systems only. The studies demonstrate the viability of OCT as a useful tool in dental medicine practice, as well as in research. Being completely non-invasive, OCT can be extended to soft tissue. Both TD and SD implementations prove the unique capabilities of OCT. For handheld scanning devices it is expected that the swept source principle (as one of the SD possibilities) will prevail, due to its high speed that allows for the reduction of distorting effects caused by the involuntary movements of the hand and of the patient. For high transversal resolution investigations, especially in more research oriented studies, it is expected that *en-face* TD-OCT will continue to coexist with SD-OCT methods, offering additionally a low cost quick provision of *en-face* view and compatibility with dynamic focus. Dynamic focus, that is the simultaneous adjustment of focus and coherence gate in depth is incompatible with SD-OCT methods and require repetitions of acquisitions under different focus in order to improve the transversal resolution, or more complex heads with division of the optical path in the object arm along different focus adjustments. In this respect, *en-face* TD-OCT provides a lower cost alternative to high transversal resolution of static samples.

We have shown that complementary studies are possible embracing OCT with more traditional methods, such as confocal microscopy and microCT. Combination of principles is expected to evolve due to their limitations when considered separately.

Key words: dentistry; non-invasive investigations; biomedical imaging; optical coherence tomography.

Corresponding author: Silvana Canjau, e-mail: canjau.silvana@umft.ro

Russian

Оптическая когерентная томография для неинвазивных исследований *ex vivo* в стоматологии — собственный опыт группы

Данный обзор посвящен результатам исследований *ex vivo* структур полости рта с помощью оптической когерентной томографии (ОКТ), которые демонстрируют огромный потенциал технологии для прижизненной визуализации тканей полости рта. ОКТ-технология может создавать высокоразрешающие кросс-секционные и анфасные изображения внутренней архитектуры исследуемых образцов (глубиной до 2–3 мм). Для этой цели используются анфасные системы с временным и спектральным сканированием. В обзоре рассмотрены возможности оценки с помощью ОКТ различных стоматологических процессов: стоматологической абфракции и стирания, дефектов материалов и микроутечки в зоне контакта пломбы и зуба, диска височно-нижнечелюстного сустава, качества крепления брекетов к твердой ткани зубов, ортопедической реставрации и микроутечки в месте контакта протеза, корневых каналов, наличия или отсутствия верхушечных микроутечек, а также контактного остеогенеза зубных имплантатов и материалов для костной пластики. ОКТ показывает внутренние особенности исследуемого материала с большей чувствительностью, чем другие существующие диагностические методы.

Обзор отражает главным образом опыт исследований нашей группы и представляет изображения, полученные с помощью нашей ОКТ-системы. Исследования демонстрируют эффективность ОКТ как полезного метода в стоматологической практике, а также в научных исследованиях. Поскольку ОКТ является неинвазивным методом, ее можно использовать для мягких тканей. Использование как временного, так и спектрального сканирования области подтверждает уникальные возможности ОКТ. Предполагается, что для переносных приборов принцип перестраиваемого лазера (как одна из возможностей спектральной ОКТ) будет преобладать ввиду его высокой скорости, которая позволяет уменьшить искажающие эффекты, вызванные непроизвольными движениями кисти исследователя и движениями пациента. Для исследования поперечных срезов с высокой разрешающей способностью, особенно в научно-ориентированных исследованиях, предполагается, что анфасная ОКТ в пространственно-временной области продолжит сосуществовать со спиральными ОКТ-методами, дополнительно предлагая низкозатратную быструю анфасную визуализацию и совместимость с динамическим фокусом. Динамический фокус, т.е. одновременная регулировка фокуса и зоны когерентности по глубине, несовместим со спиральной ОКТ и требует повторных изображений с разным фокусом, для того чтобы улучшить поперечное разрешение, или более сложных наконечников с делением оптического пути в предметном плече между путями с разными настройками положения фокуса. В этом отношении анфасная ОКТ в пространственно-временной области представляет собой более дешевый способ получения изображений с высоким поперечным разрешением для статических образцов.

Мы показали, что возможны взаимно дополняющие исследования, охватывающие ОКТ и более традиционные методы, такие как конфокальная микроскопия и микрокомпьютерная томография. Предполагается, что в дальнейшем получат развитие методы, основанные на сочетании этих принципов, так как использование по отдельности ограничивает их применение.

Ключевые слова: стоматология; неинвазивные исследования; биомедицинская визуализация; оптическая когерентная томография.

OCT systems. In the past decades, optical coherence tomography (OCT) evolved to become a powerful technique for imaging of transparent and translucent structures [1–3]. OCT is based on low-coherence interferometry (LCI), which can achieve micron-scale depth resolved quantification. The first LCI application in the biomedical optics involved the measurement of the eye length [4]. An LCI system is generally based on a two-beam interferometer. Application of such an interferometer to deliver A-scans was facilitated by a technical advantage: when moving the mirror in the reference path of the interferometer, not only is the depth scanned, but a carrier is also generated. The carrier frequency shift is Doppler shifted due to the longitudinal scanner itself. Adding lateral or angular scanning of the optical beam across the target, thin section slices can be achieved non-touch and with high axial resolution [5].

En-face time domain OCT (TD-OCT). Collecting many A-scans from various adjacent transverse positions generates B-scan images. The lines in the raster generated correspond to A-scans and are oriented along the depth coordinate. B-scan images can also be produced from T-scans at different depths. In the case of these T-scans, the transversal scanner produces the fast lines in the image [6–8], by controlling either the transverse scanner along the X-coordinate (horizontal), along the Y-coordinate (vertical) or along a polar angle θ, while the other two scanners remain fixed. This procedure has a clear advantage in comparison with the A-scan based B-scan procedure as it allows for the production of OCT transverse (or *en-face*) images for a fixed reference path; such images are called C-scans.

For TD-OCT the path length of the reference arm is scanned in time. Interference (i.e., the series of dark and bright fringes) is only achieved when the optical path difference (OPD) lies within the coherence length of the optical source. The envelope of this modulation changes as the OPD is varied; the peak of the envelope corresponds to the path length matching [9–11].

The schematic diagram of the *en-face* TD-OCT system used in our studies is depicted in Figure 1. The optical source (OS) employed in this regime of operation was a pigtailed superluminescent diode (SLD) emitting at 1300 nm and with a spectral bandwidths of 65 nm. This determines an OCT longitudinal resolution of 8.6 μm in teeth. Depending on the ratio between the focal lengths of lenses L_3 and L_4, the lateral resolution and maximum achievable lateral

Silvana Canjau, Carmen Todea, Meda Lavinia Negrutiu, Cosmin Sinescu, ..., Adrian Gh. Podoleanu

Figure 1. Combined OCT/confocal imaging system anatomy. The OCT channel can operate either as an *en-face* TD-OCT or as a SS-OCT system. OS: optical source (broadband source for the *en-face* TD-OCT and swept source for SS-OCT); SLD: superluminescent diode; SX, SY: galvoscanners; APD: avalanche photodiode; L_{1-4}: achromatic lenses; MO_{1-5}: microscope objectives; BS_1: dichroic beam-splitter; BS_2: beam-splitter (20/80); LPF: low pass filter; TS: translation stage; $M_{1,2}$: flat mirrors; $DC_{1,2}$: directional couplers; BPD: balanced photo-detector (200 kHz bandwidth for *en-face* TD-OCT and 200 MHz for SS-OCT)
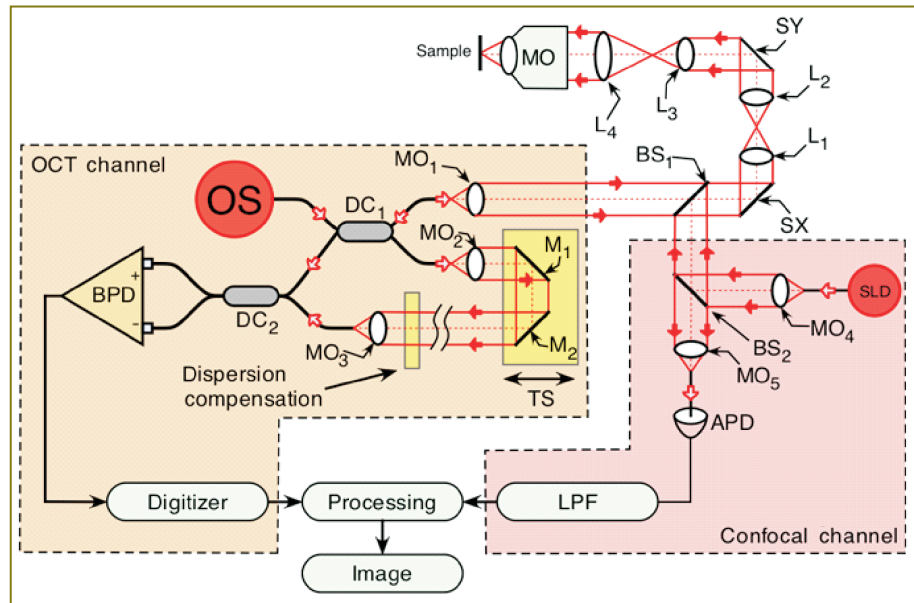
size of the *en-face* images can be tweaked. We used two configurations:

(i) Low numerical aperture (NA) interface optics, which allows 1 cm lateral image size.

(ii) High NA interface optics with a maximum 1 mm lateral image size.

In addition to the OCT channel, the imaging system is equipped with a confocal channel using as light source a second SLD emitting at 970 nm. This channel was used in some of the investigations to guide the adjustment of the sample as well as to provide some complementary reflectivity measurements.

Light from the OS is injected into the system via a first directional coupler (DC_1), which splits the light toward the two arms of the interferometer, the probing and reference arms respectively. The probing beam is reflected by the dichroic beam-splitter (BS_1) and then sent via the galvanometer scanners SX and SY towards the sample. BS_1 is a hot mirror that reflects light of wavelengths longer than 1 µm. Two telescopes incorporated between these elements conveniently alter the diameter of the beam to match the aperture of different elements in the probing path and convey a probing beam of 8 mm in diameter through the microscope objective (MO) pupil plane when a high resolution mode is required. The two transverse scanners SX and SY are separated here using telescopes to project a flat wave front on the target under high NA. Lenses L_1, L_2, and L_4 have focal lengths of 7.5 cm, while lens L_3 has a focal length of 3 cm. The MO is a scan lens (focal length 1.8 cm) to prevent image degradation and distortion during scanning. Hence a lateral resolution of around 2 µm was experimentally measured in the confocal channel and better than 5 µm in the OCT channel. Light backscattered by the sample passes a second time through the object arm and is guided via the DC_1 toward the second single mode directional coupler (DC_2), where it interferes with the light coming from the reference arm. Both output fibers from the

second coupler are connected to two pin photo-detectors in a balanced photo-detection (BPD) unit. After digitization, the OCT signal is rectified and low-pass filtered in the processing block.

The confocal channel operates at a different wavelength than that of the OCT, to allow the utilization of a high gain silicon avalanche photodiode (APD). The light from the SLD at 970 nm is collimated by a MO_4 and reflected by a beam-splitter (BS_2) (20% reflection) toward BS_1. Light at 970 nm is transmitted via BS_1 and BS_2 toward the APD. The photo-detected signal is amplified and low-pass filtered in LPF. A computer-driven translation stage (TS) is used to alter the reference path length in order to acquire C-scan image frames from different depths and thus to provide depth scanning in the B-scan regime.

The scanning procedure is similar to that used in any confocal microscope, where the fast scanning is *en-face* (line rate, using the galvanometer scanner SX) and the frame scanning is much slower (at the frame rate, using the galvanometer scanner SY) [12]. The frame grabber in Figure 1 is controlled by signals from the generators driving SX and SY galvanometer scanners. The SX galvanometer scanner is driven with a ramp at 500 Hz and the SY galvanometer scanner with a ramp at 2 Hz. In this way, an *en-face* image, in the plane (X, Y) is generated at constant depth. The next *en-face* image at a new depth is then generated by moving the TS in the reference arm of the interferometer and by repeating the (X, Y) scan. Ideally, the depth interval between successive frames should be much smaller than the system resolution in depth, and the depth change is applied only after the entire *en-face* image has been collected. However, in practice, to speed up the acquisition, the TS was moved continuously.

To construct B-scan images, no signal is applied to the frame scanner, while the line scanner is driven with the same signal as in the C-scanning regime, and the TS is moved along the optical axis of the reference beam. In this

case, the frame grabber is controlled by signals from the generator driving the SX (or the SY) with a ramp at 500 Hz, and TS is moved over the depth range required in 0.5 s. Thus, an OCT cross section image is produced either in the plane (X, Z) or (Y, Z).

In the images presented in this manuscript, no other phase modulation was employed apart from that introduced by the galvanometer scanner [6, 8] determining the line in the raster.

In the low NA configuration, L_3 and L_4 have been removed, only a single optical component being placed between the SX, SY and the sample (MO, focal length 4 cm) allowing a larger lateral size image. Consequently, the transversal resolution was reduced to 15 μm.

Spectral domain OCT (SD-OCT). In SD-OCT, the spectrum at the output of the LCI is measured. A Fourier transformation of the acquired spectrum delivers an A-scan, without any movement in the reference arm [13–16]. Due to the fact that all depths are obtained in one measurement, the speed of producing B-scan images improves dramatically, as well as the signal-to-noise ratio in comparison to TD-OCT. As drawbacks, SD-OCT cannot provide a faster production of *en-face* images or axial ranges longer than those achievable in TD-OCT. SD-OCT can be implemented in two ways: swept source OCT (SS-OCT) and camera based, or spectrometer based (Sp-OCT). In some papers, one or both of these methods are referred to as Fourier domain OCT methods. Both types of methods have been employed in instruments we have assembled, we show here results obtained using the SS-OCT principle only.

A SS-OCT instrument was assembled, with a diagram similar to that used for TD-OCT (See Figure 1). In this case the OS is a fast SS and the photo-detector is changed to a faster one (over 200 MHz instead of 400 kHz). The SS is from Axsun Technologies Ltd. (central wavelength 1060 nm, sweeping range of 106 nm (measured at 10 dB), average output power of 16 mW, sweeping rate 100 kHz). A depth resolution determined by the SS tuning range of 12 μm in air was experimentally measured. The SS-OCT system was used in a low NA configuration; hence a lateral resolution of ~14 μm was experimentally measured. The optical power on the sample is 3.6 mW. The DC_2 output signals are sent to a fast balanced photo-detector BPD (model PDB460C, bandwidth 200 MHz, Thorlabs, Inc., USA). A 12-bit analog-to-digital acquisition card digitized the output of the photo-detector (Alazartech ATS9350, Canada), while an "in-house" LabVIEW (National Instruments, USA) created software is used to produce, display, and record the images. The lateral size of the 3D images, determined by the amplitude of the voltages applied to the galvoscanners and the focal length of MO, is 4.4×4.4 mm, while their axial size, determined by the SS and the digitizer is 3.7 mm. The system is able to produce 500×640 pixels B-scan images (cross-sectional images of the sample) at a frame rate of 100 Hz. 3D reconstructed images of 500×500×640 pixels could then be produced. The inspection of the volume can be performed either along B-scans or C-scans. As 500 A-scans are used to construct each B-scan image, given the sweeping speed of the SS, a number of 100 B-scans are acquired per second. Hence, in order to acquire data to reconstruct a 3D volume made of 500 B-scans, 2.5 s are needed.

A Sp-OCT was also assembled, operated at 840 nm using an Aviva camera (Atmel, USA) at 29 kHz line rate. It was used in a single study here, to produce B-scans only, therefore its diagram is not shown. Interested readers can find more data in [17].

The various OCT applications in dentistry tested by our research group will be presented, considering each investigated structure at a time. The imaging systems, as presented above have been used at different stages of our research activity, in line with the OCT progress from TD-OCT towards SD-OCT methods. Compared with TD-OCT, SD-OCT methods present the advantage of increased phase stability for functional imaging. However, SD-OCT methods exhibit three main disadvantages: decay of sensitivity with OPD, impossibility to move the focus to the depth investigated while scanning and symmetric (ghost) images if the OPD=0 position crosses the object volume, problem known as mirror terms. The impossibility of focusing at selected depths renders the technology unsuitable to high transversal resolution microscopy, where TD-OCT is favored. If minute details are to be identified in the sample, then TD-OCT is better. In addition, *en-face* TD-OCT can deliver an *en-face* image direct, while even the fastest SD-OCT systems known today still need several seconds to acquire all data volume and produce the *en-face* image by software means. In case large size images are to be generated from soft moving tissue, then SD-OCT methods should be used for its higher speed.

Clinical results. In dentistry, current scientific literature shows that OCT has been successfully used for acquiring images of: dental biofilm [18, 19], attrited teeth [20], enamel erosion [21], dentin structures [22–25], vertical root fractures [26–27], and incipient carious lesions [28–46]. It was also used for the evaluation of severity in advanced carious lesions [47] and re-mineralization of root caries [48], dentin re-mineralization [49–50], lesion progress in root caries [51], for quantification of re-mineralization [52–57], as well as for determining the efficiency of different agents in the inhibition of demineralization [52, 58–64]. Additionally, several research groups have demonstrated that OCT is capable to evaluate the oral mucosa [65–67], the micro-leakages and internal defects of composite restorations [68–81], dental sealants [82–84] and endodontic fillings, the root internal structure [85, 86], the dental implant-abutment interface [87], and dental adhesives [88]. OCT is able to identify early signs of inflammation, unlikely to be detected by clinical examination. OCT imaging offers the exciting potential to detect peri-implantitis before significant osseous destruction occurs [89]. OCT has also been employed for periodontal diagnosis [90], for evaluating the integrity of dental prosthesis, their quality [91], their marginal fitting [30, 47, 92, 93] and their adhesion to the tooth structure [94, 95], for monitoring the periodontal ligament changes induced by orthodontic forces [96, 97], and orthodontic interfaces [98–101].

Hard dental tissue (noncarious lesions)
Occlusal overload. Occlusal overload represents a major concern to dentists because of its undesired consequences,
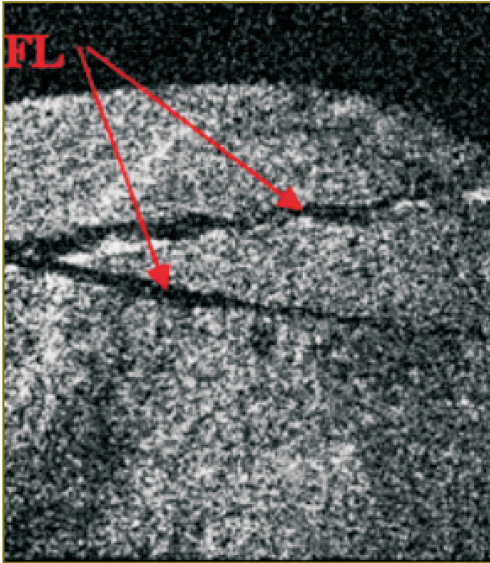
Figure 2. Fracture lines (FL) in enamel, a zoom approach in an occlusal overloaded anterior tooth, with a normal crown morphology at 0.4 mm inside (measured in air) and 6 mm lateral size. Reproduced with permission of the say it, OSA, SPIE [103]

which include excessive tooth wear (pathological attrition and abfractions), dental crown and/or root fracture, failure of dental restorations, and temporo-mandibular disorders. An early diagnosis is essential in such cases. Our group has demonstrated that OCT represents a promising, non-invasive alternative technique for early detection and monitoring of occlusal overload in bruxing patients [102–104]. *En-face* TD-OCT and fluorescence microscopy were used to investigate the wear of anterior teeth derived from young patients with active bruxism (strong, unconscious, and rhythmic grinding and/or clenching of teeth during the day or during the sleep [105], mainly caused by high levels

of emotional stress and by occlusal interferences during protrusive or laterotrusive mandibular movements) [103]. The teeth presented first-degree pathological wear established through a tooth wear index (TWI), which was proposed by Smith and Knight in 1984 in order to score the wear of all four visible dental surfaces [106]. In our study the TWI score equals 1 (showing loss of enamel surface characteristics without exposing dentine, with a minimal loss of contour). The combination of information collected by OCT and fluorescence microscopy revealed a characteristic pattern of enamel cracks that reached the tooth surface.

En-face TD-OCT was also used to investigate extracted anterior teeth with a normal crown morphology (without pathological attrition), which derived both from patients with active first-degree bruxism diagnosed by using BiteStrip devices and from subjects without parafunction [103]. The teeth from non-bruxing patients revealed a homogenous structure of the superficial enamel on the *en-face* TD-OCT images. Despite the normal crown morphology, the teeth extracted from patients with first-degree bruxism showed signs of enamel damage in the OCT images. This consisted of a characteristic pattern of cracks, which did not reach the tooth surface (Figure 2).

Abfraction and attrition. The evolution of the pathological dental wear over time is essential for the prognosis of teeth and for the initiation of the most suitable therapeutic steps. Monitoring these lesions helps to determine whether a particular phenomenon is progressive or not.

Our research team demonstrated microstructural characterization of abfraction by *en-face* TD-OCT [107, 108]. The investigation of bicuspids with normal crown morphology revealed a homogenous structure of the buccal cervical enamel. Occlusal-overloaded bicuspids (derived from patients with active bruxism) were imaged by the system in Figure 1, which produced constant depth OCT images (C-scans) as well as cross cross-section OCT images (B-scans). These images revealed the wedge-shape loss of cervical enamel and the damage of the underlying dentin. The high-occlusal forces produced a characteristic
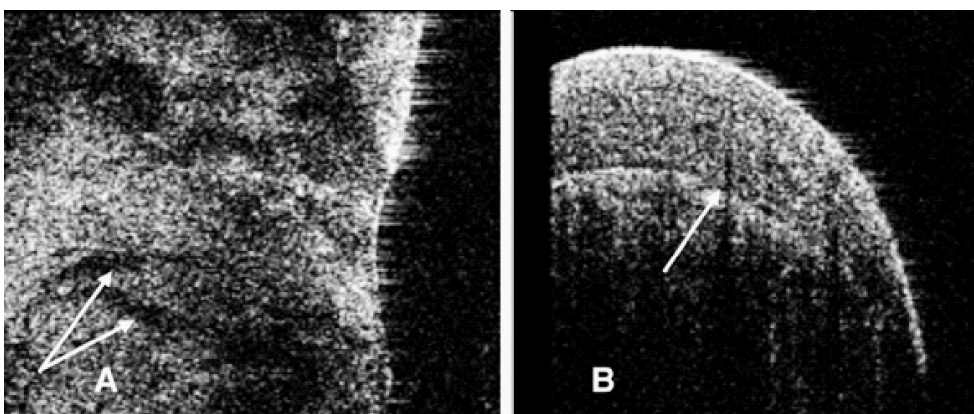
Figure 3. OCT images of a sample of occlusal overloaded bicuspid: (A) C-scan image revealing the cracks that are penetrating the cervical dentine, reaching the surface of the abfraction (lateral image size 4×4 mm, at a depth of 910 μm from the top measured in air); (B) B-scan image of the same microstructural defects (image size 4×4 mm; 2.5 mm in air). Reproduced with permission of the say it, OSA, SPIE, etc. [108]
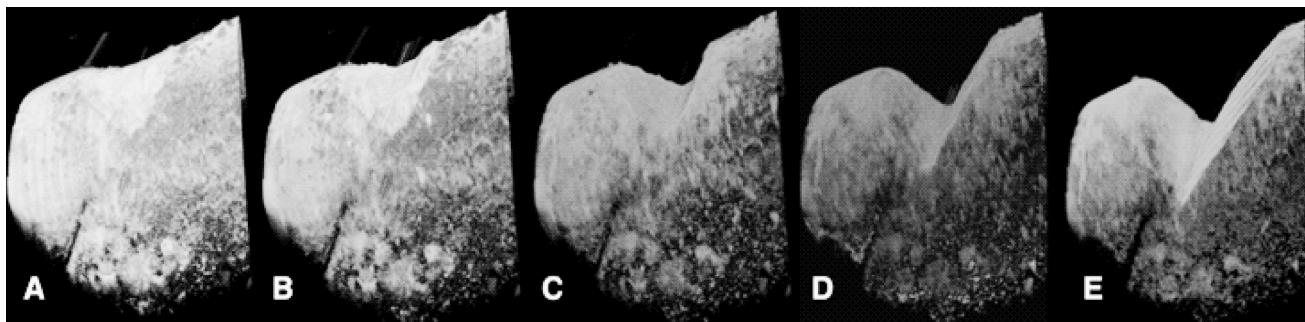
Figure 4. 3D reconstructions of the vestibular cervical areas of a premolar sample, where abfraction usually appears: (A) the initial area with no modification; (B)–(E) after different levels of abfraction evolution. The size of the volumes is 3.2×3.2 (lateral)×2.7 mm (depth measured in air). Reproduced with permission of the copyright owner [110]
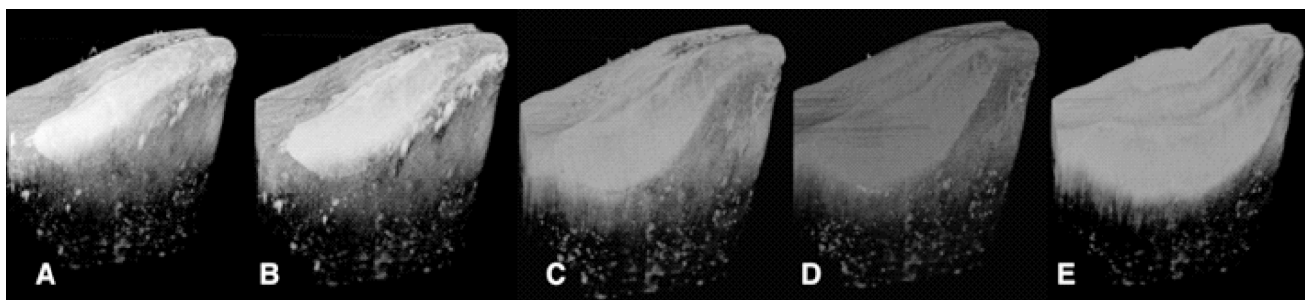
Figure 5. 3D reconstructions of the incisal parts of the incisors where the attrition was induced: (A) the initial volume with no modification; (B)–(E) after different levels of attrition evolution. The size of the volumes is 3.2×3.2 (lateral)×2.7 mm (depth measured in air). Reproduced with permission of the copyright owner [111]

pattern of large cracks, which reached the tooth surface (Figure 3).

In other studies from our group [109–111], artificially induced defects (attrition and abfractions) in teeth were similar to those observed in the clinic (scored by the TWI in terms of enamel and dentine loss). The loss of dental hard tissue can be qualitatively evaluated by inspecting either two-dimensional images or 3D reconstruction of volumes. Our study has shown that a more accurate figure on evaluation of such processes is provided by 3D reconstructions, as individual B-scans may show less loss. When the 3D reconstruction was considered, the maximum depths of the abfractions were larger than the values measured in some individual B-scan images, leading to: 0.41 mm (Figure 4 (C)), 0.98 mm (Figure 4 (D)), and 1.173 mm (Figure 4 (E)). Using the 3D reconstructions of the attritions, again, the maximum depth values obtained were different from the values measured on the B-scan images: 0.33 mm (Figure 5 (B)), 0.67 mm (Figure 5 (C)), 0.83 mm (Figure 5 (D)), and 1.083 mm (Figure 5 (E)). The OCT system used for this study presented a minimum volume detectable change in the sample of ~2352 μm^3.

The amount of hard dental tissue lost, as well as the evolution of such loss is important. Providing these two pieces of information constitutes a useful guidance for the clinical evaluation of abfraction and attrition.

Another major advantage of this technology is provided by the speed of acquisition, more than 100 times faster than the TD-OCT used in our previous studies [102–104]. The method is equally applicable to faster systems working at over 1-MHz line rate [112, 113]. A high-speed SS-OCT may therefore prove a more suitable clinical tool to quantify abfraction and attrition.

Dental fillings. *En-face* TD-OCT shows promise in the examination of structural quality of these restorations. In several of our preliminary studies, amalgam [114], composite resin [115–118], and compomer [119] have been used to restore teeth. The amalgam (by virtue of its metallic composition) completely obscures the tooth interior beneath it in any OCT image. However, the other two materials, by virtue of their small absorption coefficients, allow for the visualization of internal landmarks such as the dental enamel junction in the tomogram (Figure 6), obtained with the system in Figure 1 [120].

OCT is limited in the capability of separating the interfaces between the adhesive layer, the dental tissue and the resin; the adhesive layer cannot sometimes be told apart from air gaps. The issue is that interfaces between different materials are detected in OCT based on the difference between their indices of refraction [30], and the tooth adhesives present a quite low refractive index. Therefore, in order to better visualize such challenging interfaces, we proposed to employ materials that dope the adhesive to strengthen the backscattered light [121, 122]. In a recent study [123], the procedure of enhancing the contrast in the OCT image by applying an optimum concentration of zirconia to the

adhesive layer was evaluated. This procedure allowed better visualization of the integrity of the adhesive fillings, by enhancing the interfaces between the adhesive and the tooth structures and between the adhesive and the composite resin.

Endodontic treatment. The quality of endodontic treatments and root canal fillings were investigated with *en-face* TD-OCT technology [124–129]. It was possible to identify areas of apical micro-leakage between the filling material of the root canal space, the gutta-percha cones, and the root canal walls (Figures 7 and 8). For a better assessment of the quality of the endodontic treatment, the system equipped with a second channel, confocal, for guidance (as shown in Figure 1) was employed. This set-up provides both dual imaging and magnified view. The confocal image aids guidance and allows for focus adjustment in the OCT investigation. In order to obtain the images, sections up to a depth of 2 mm were scanned (Figure 9), thus quantifying the level at which defects appeared within the filling material or between the filling material and the gutta-percha material. During the examination, it has been evidenced that in some samples,
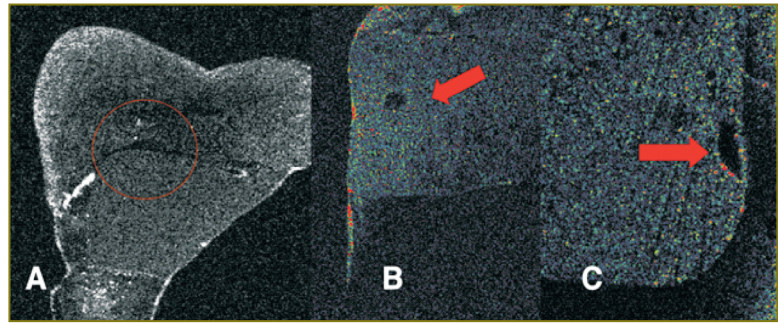
Figure 6. (A), (B) and (C) 4×4 mm lateral size, slice from a depth of 500 μm measured in air. Coronal micro-leakage is detected between the restorative material and the tooth structure. Also, voids of different sizes are present inside the restorative material

defects were present in all sections to a full depth of 2 mm, while in others defects were observed in fewer layers. This observation allowed for a quantitative statistical analysis based on the number of sections in which defects were present.

In a different study [130], we employed OCT to investigate the fitting and the gap width between fiber posts, adhesive luting cement and root canal wall. The results obtained have

Figure 7. 3D reconstruction of the apical microleakage area using a stack of 44 C-scan images acquired at a differential depth of 10 μm measured in air; *a*: gutta-percha cone, *b*: root canal sealer, *c*: root canal walls, *d*: microleakage area
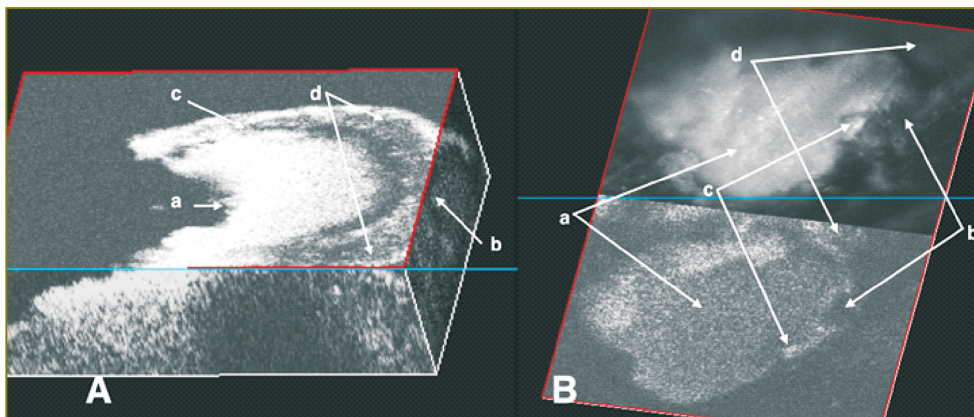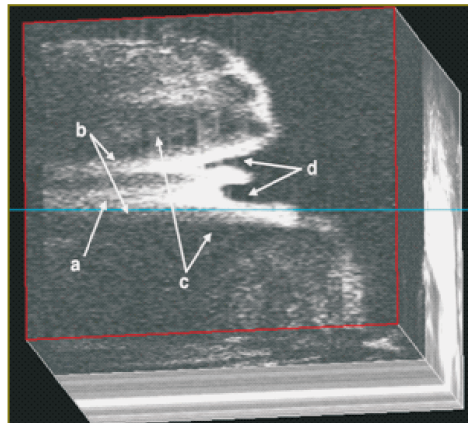
Figure 8. (A) and (B) OCT image of root canal apical microleakage; *a*: guta-percha cone, *b*: microleakage space, *c*: root canal sealer, *d*: root canal walls
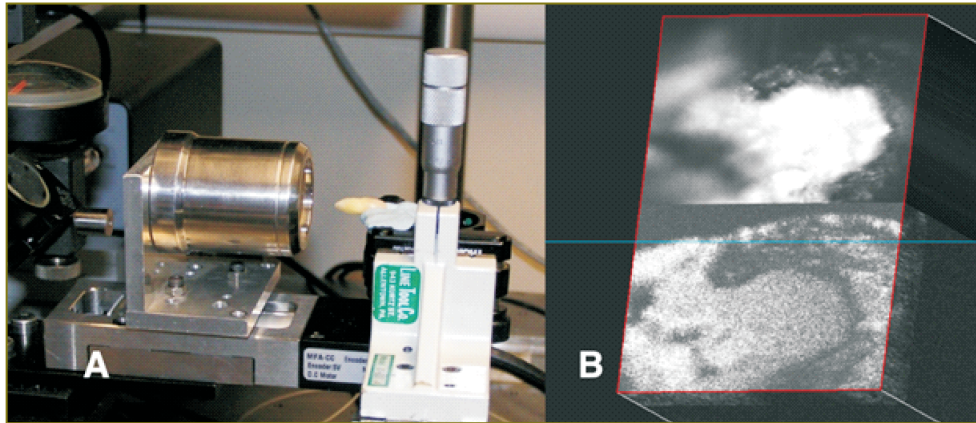
Figure 9. Investigation of the same root canal filling, using the dual *en-face* TD-OCT/CM. (A) Photograph of tooth in front of the scanning head; (B) a pair of confocal image (top) and *en-face* OCT image (bottom). Reproduced with permission of the copyright owner [129]
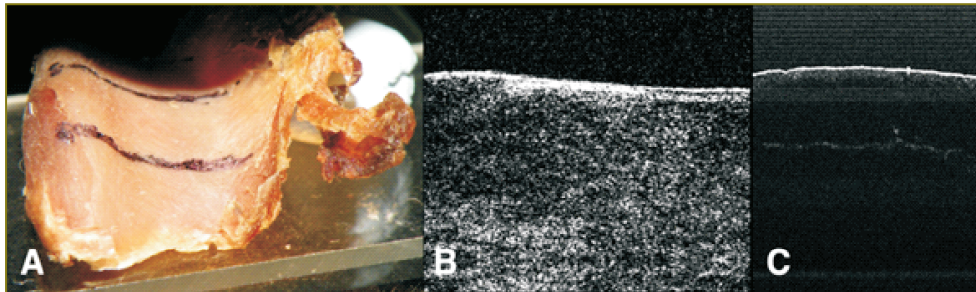
Figure 10. OCT investigation of pars posterior of the temporo-mandibular joint disc: (A) investigated area (between the black lines); (B) C-scan *en-face* OCT image (lateral image size 4×4 mm) at a depth of 800 microns from the top measured in air: due to the tilt of the disc surface, black is air and below white border is the tissue; the white superficial layer covers a disc tissue with homogeneous microstructure; (C) B-scan SD-OCT image: the white superficial layer is identified better than the underlying disc tissues — lateral image size 4 mm (horizontal), axial size 1 mm measured in air (vertical). Reproduced with permission of the copyright owner [131]

proven the importance of assessing the interface quality of the fiber post, adhesive luting cement and root canal wall after each fiber post luting process.

Temporo-mandibular joint disc. In a preliminary study [131], we revealed the micro-structural characterization of the temporo-mandibular disc by using both *en-face* TD-OCT and SD-OCT. 8 human temporo-mandibular joint discs were harvested from dead subjects, having less than 40 years of age; the samples were then conserved in formalin. They presented normal morphology, with thicker posterior pars (2.6 mm on the average) and thinner intermedia pars (1 mm on the average). The OCT investigation of the healthy temporo-mandibular joint discs revealed their homogeneous microstructure, covered by a white superficial layer (Figure 10). The longer wavelength of the TD-OCT assembled offers a larger penetration depth (2.5 mm in air) than that achievable in the Sp-OCT system (1.5 mm), which is important for the analysis of the pars posterior, while the Sp-OCT proved to be much faster.

The longer wavelength of the TD-OCT allowed better identification of the homogenous microstructure of the thicker posterior pars on C-scan images; a continuous white superficial layer of a proteoglycan could also be visualized at 1300 nm. The detailed observation was allowed by the TD-OCT method, compatible with dynamic focus.

Orthodontics. The *en-face* TD-OCT system shown in Figure 1 was also used in our studies to evaluate the connection between the bracket and the tooth structure [132]. Orthodontic attachments bonding strength cannot be measured with OCT; however, identifying and visualizing the voids in the composite can provide some indication on the quality of the bonding [133, 134]. OCT investigations provide information on the micro-leakage of the bracket's bonding; in Figure 11 (A), several gaps can be seen along the bracket base. Also, it was possible to identify a lack of adhesive material on the side of the bracket (Figure 11 (B)). Although this work was restricted so far to *ex vivo* investigations [135, 136], the tooth-bracket interfaces could also be imaged *in vivo* by assembling special hand held probes as described in [137].

Implantology. Bone grafting is a commonly performed surgical procedure for bone regeneration in a variety of orthopaedic and maxillofacial procedures. There are several aspects that require attention when implementing this type

of procedures, such as consideration of materials used in bone regeneration, quality control methods, adjustment of the initial bone regenerative scaffold, monitoring of their osteoconduction and osteo-integration period, and biomedical evaluation of the new regenerated bone. It would be valuable to extend the OCT evaluation of the bone grafting material/bone interface to a wide area of hard tissue augmentation procedures. The quality of bone grafting was evaluated by using TD-OCT (Figure 12) and validated by using microCT (Figure 13). Based on these studies, it becomes easier to extend OCT to *in vivo* evaluations to provide qualitative and quantitative data on the bone augmentation procedures [138–140].

The quality of the implant insertion can be investigated by using the analysis of the interface between the implant and the bone. We have initiated two studies on the numerical simulation and tensional stamps. Both have demonstrated that *en-face* TD-OCT is able to evaluate the morphology of interfaces between the implant and the bone [141, 142]. Both C-scan and B-scan OCT images were collected. 3D analysis was made possible by acquiring a number of 30 to 100 C-scans that were used post-acquisition to
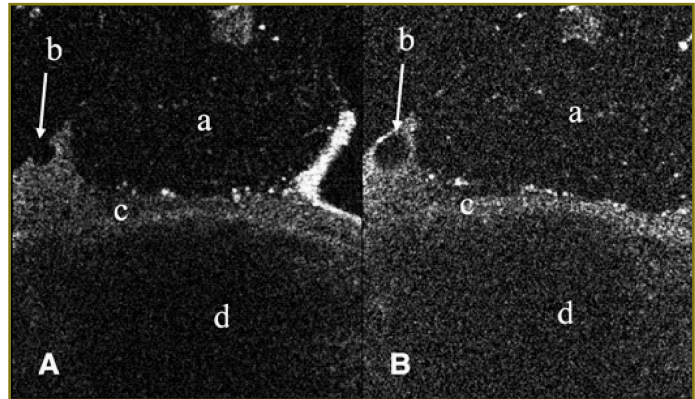
Figure 11. (A) C-scan image of an adhesive bracket bonded on a vestibular maxillary premolar area. Part *a*: ceramic bracket; part *b*: gap trapped inside the adhesive resin between the bracket and the tooth; part *c*: adhesive resin layer; and part *d*: buccal area of the maxillary premolar. Depth measured in air: 60 µm. Lateral size: 4.4 mm. (B) Adhesive bracket bonded on a vestibular maxillary premolar area. Part *a*: ceramic bracket; part *b*: lack of adhesive layer material in a large area between the bracket and the tooth; part *c*: adhesive resin layer; and part *d*: the vestibular area of the maxillary premolar. Depth from top, 160 µm measured in air. Lateral size: 4.4 mm. Reproduced with permission of the copyright owner [132, 135]
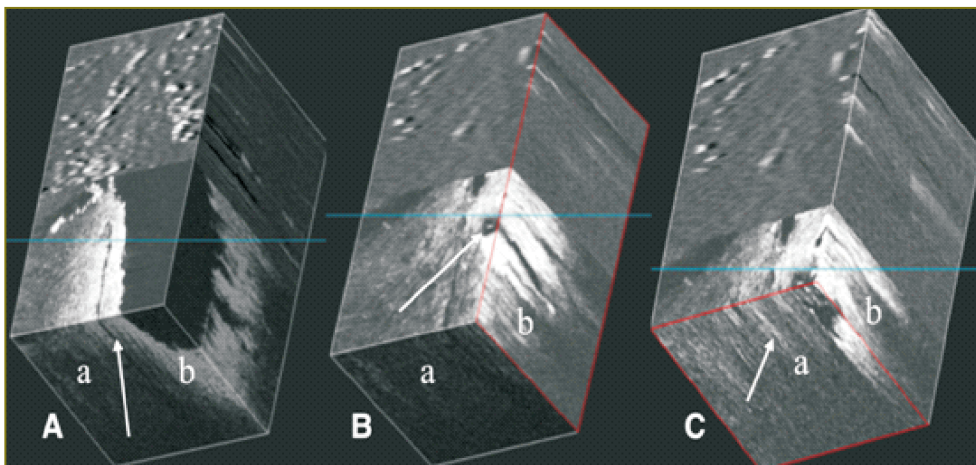
Figure 12. 3D reconstruction of TD-OCT investigated sample — 3 months from the augmentation with bone substitutes; *a*: rat bone, *b*: bone substitute. (A) Good delimitation between the bone and the bone substitute; (B) the opening of the gap affects the interface allowing to form a reactive space between the bone and the bone substitute; (C) at deeper level — no delimitation at the interface between the bone and the bone substitute. Reproduced with permission of the copyright owner [138]

Figure 13. MicroCT at three months after bone augmentation procedure; *a*: the remaining regenerative materials (white color) can be separated from *b* the normal bone (dark blue) and *c* the new bone (light blue). Reproduced with permission of the copyright owner [139]
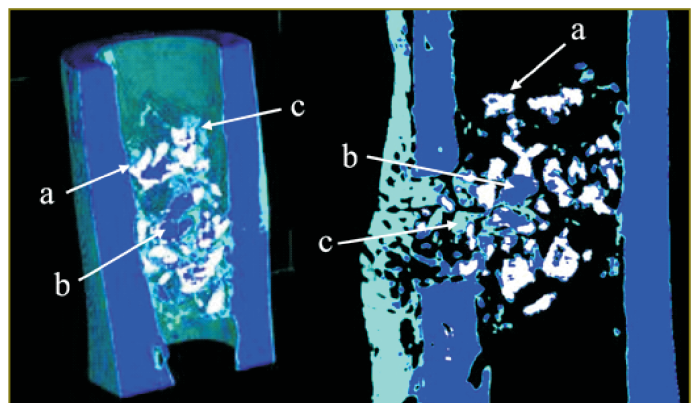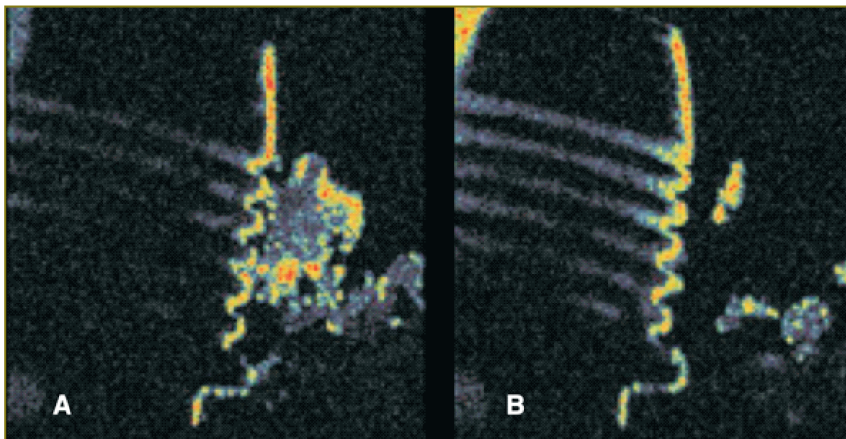
Figure 14. C-scan OCT images (two-dimensional *en-face*) showing details from the interface between implant 4 and mandible bone (A) and (B) show major defects in the distal part of the implant. Slide 19 (A), 37 (B) from 61 slices acquired from a 2 mm depth measured in air, lateral size: 18 degree, distance between slices 33 microns measured in air. Reproduced with permission of the copyright owner [141]

explore the volume of the tissue around these interfaces. The authors chose to evaluate the implant-supported restorations on two implants connected with conjunction bars and the implant supported restorations on four implants connected with a bar.

For the model development we used the ANSYS Computer-Aided Engineering (CAE) software. The ANSYS CAE software program was used in conjunction with a 3D Computer-Aided Design (CAD) to simulate the behavior of mechanical parts under thermal/structural loading conditions. ANSYS automated Finite Element Analysis (FEA) technologies from ANSYS, Inc. (USA) were used to generate the results listed in this report. Numerical simulation investigations generated specific charts that allowed for the quantitative evaluation of the tensions around the implants and in the bone structure. The micro measurement method was used to validate the results obtained using the numerical simulations. It was demonstrated that the four implants configuration with a connecting bar is better than the solution of two implants with a connecting bar because the tensions in the implant bone interfaces are lower. The most important feature is represented by the intimate contact between the implant and the bone. To investigate such aspects, it is again essential to employ a non-invasive method to predict the stability of the inserted implants. *En-face* TD-OCT images from different interfaces between mandible bone and the implants are shown in Figure 14. Using occlusal scanning, numerous spaces between the implant and the bone were found. These can be the source of deficient biomechanical behaviour of the implant-supported restoration. The classical investigation methods like nuclear magnetic resonance and computed tomography are invasive and they exhibit inferior resolution. Therefore these methods cannot ensure a good prognostic of the dental treatment, while OCT is capable to achieve better overall resolutions while being non-invasive.

Prosthodontics. Sequential and rapid switching between the *en-face* regime and the cross-section regime, specific

for the *en-face* TD-OCT technology represents a significant advantage in the non-invasive examination of dental prostheses [120, 143–158]. Several types of such prostheses were investigated, including metal-ceramic fixed partial prostheses, metal-ceramic crowns, metal-polymer fixed partial prostheses, metal-polymer crowns, polymer and all-ceramic fixed partial prostheses, and complete dentures. The main goal has been to detect the presence or absence of material defects and micro-leakages at the prosthetic interfaces.

In several of the prostheses investigated by our group, defects that may cause their fracture were identified. The areas depicted in the OCT images present several small canals in the base that can be colonized in time with bacteria. Such areas can also cause the start for esthetic and functional failure of the prosthetic treatment. The defects are usually located inside the material and cannot be depicted visually or by any other conventional imagistic method. A series of these defects are illustrated in Figures 15 and 16, obtained using the *en-face* TD-OCT system.

In yet another study, we have analyzed the potential of *en-face* TD-OCT for the investigation of all-ceramic veneers immediately after the bonding process. This evaluation can be useful for establishing the prognostic of the prosthetic treatment. 32 Empress veneers (Ivoclar Vivadent, Lichtenstein) were investigated using *en-face* TD-OCT. The scanning procedure was performed vestibular, oral, mesial and distal for each sample [159]. The investigation
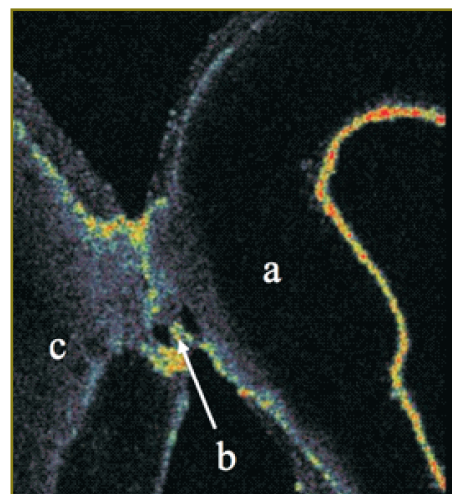
Figure 15. C-scan OCT image matching the depth of the defect at *b* approx 0.2 mm measured in air from the top, lateral size 9.5 by 9.5 mm. The image shows the interface between pillar crown *a* and pontic *c* in a metal ceramic fixed partial prosthesis. The defects inside the ceramic layers can be observed — part *b*. Reproduced with permission of the copyright owner [156]
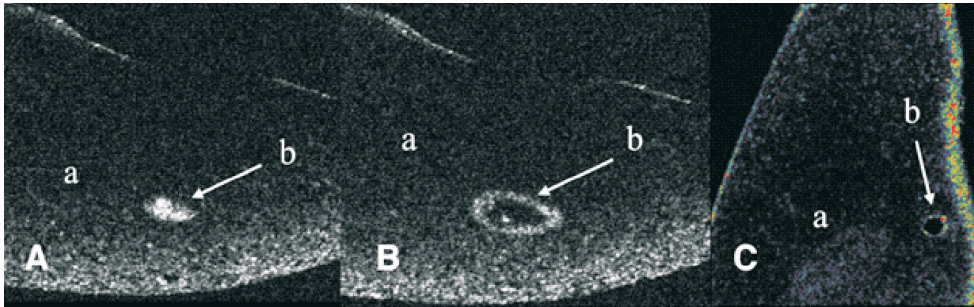
Figure 16. C-scan OCT images from esthetic fixed partial prostheses. (A) and (B) refer to the same polymer prosthesis; images are acquired from different depths and with different lateral size. (A) 140 μm from the top measured in air, with a void well defined inside the material; (C) 4.4 mm lateral size and deeper than in (A) by 100 μm. (C) All ceramic crown pressed ceramic technology. Part *a*: crown and part *b*: defect inside the ceramic layers at approximately 600 μm depth measured in air. Reproduced with permission of the copyright owner [120, 158]

revealed poor marginal adaptation for 18 out of 32 samples. The marginal adaptation problems were identified especially in the proximal and oral areas (Figure 17).

Handheld scanning probes for OCT. Several variants of handheld scanning probes for OCT were developed in our groups, in an effort to make them as light, simple and low-cost as possible. We have shown that probes can be constructed almost entirely from off-the-shelf parts and ergonomic designs, like that shown in Figure 18 [137]. This has been used for an *ex vivo* study of metalo-ceramic dental prosthesis [137].

The handheld probes devised so far employ a one-dimensional galvanometer scanner (1D GS), that provide distortion-free OCT images when driven by triangular signals [160, 161]. In contrast, Micro-electro-nechanical systems (MEMS)-based handheld probes are sinusoidally driven, using resonant oscillatory mirrors; therefore they require post-processing of OCT images in order to remove distortions [162]. Progress is under way to develop two-dimensional scanning heads to provide volumetric reconstructions of the samples investigated [163].

The 1D GS-based handheld probes developed in [137] reached a mass of 0.35 kg, in comparison to MEMS-based probes, of 0.5 kg [162] and to commercially available probes of 1.5 kg (Bioptigen Envisu, USA) or 2.2 kg (Optovue iVue, USA).

A handheld probe developed in our group has already been applied to an *in vivo* study in an ENT Department in a clinical environment [164]. The development of handheld probes is part of our effort to extend *ex vivo* to *in vivo* clinical investigations.

Conclusions. The paper presents the experience of our multidisciplinary team in acquiring OCT images using several own assembled OCT systems. Using such systems, we investigated and assessed non-destructively hard dental structures, dental materials, dental restorations and the temporal-mandibular joint disc. The studies
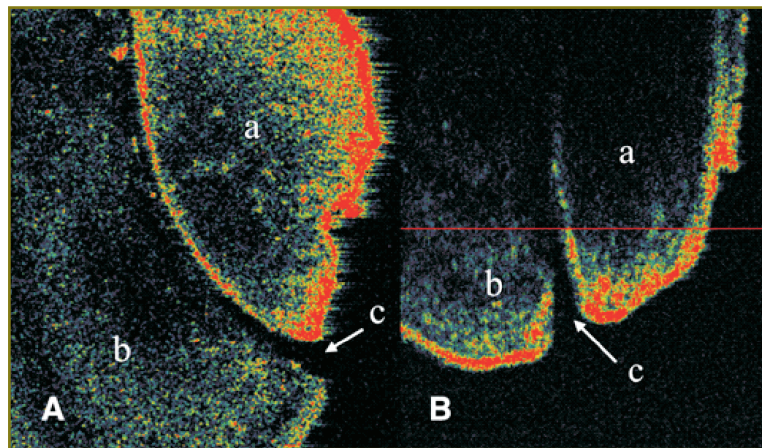
Figure 17. *a*: veneer, *b*: tooth, *c*: poor marginal adaptation on proximal area — Empress veneer: (A) C-scan, slice 23 from 94, 8 degree in air; (B) B-scan allowing to view the issues of the marginal adaptation. Reproduced with permission of the copyright owner [159]
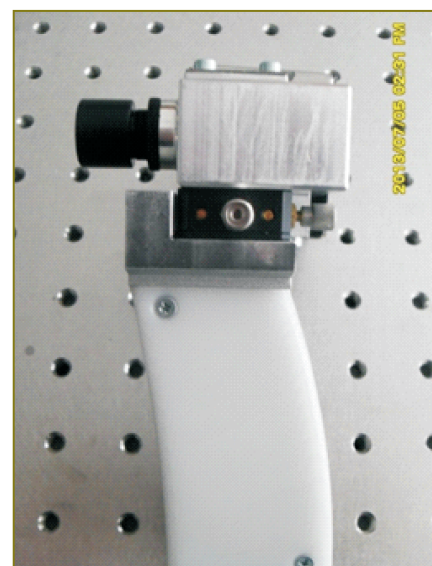
Figure 18. Handheld scanning probe — ergonomic variant [137]

demonstrate the viability of OCT as a useful tool in dental medicine practice, as well as in research. Being completely non-invasive, OCT can be extended to soft tissue. It is also expected that technological progress in the most important area for OCT applications at the moment, eye imaging, will spur collateral advancement of OCT development in dentistry. For instance, decrease in the cost of handheld devices used in imaging the anterior chamber of the eye, will impact the cost of similar systems that can be applied to dentistry with a minimum of alterations. Both TD and SD implementations prove the unique capabilities of OCT. For handheld scanning devices it is expected that the swept source principle (as one of the SD possibilities) will prevail, due to its high speed that allows reduction of distorting effects caused by involuntary movements of the hand and of the patient. However, for high transversal resolution investigations, especially in more research oriented studies, it is expected that *en-face* TD-OCT will continue to coexist with SD-OCT methods, offering additionally a low cost quick provision of *en-face* view and compatibility with dynamic focus. Dynamic focus, that is the simultaneous adjustment of focus and coherence gate in depth is incompatible with SD-OCT methods and require repetitions of acquisitions under different focus in order to improve the transversal resolution, or more complex heads with division of the optical path in the object arm along different focus adjustments. In this respect, *en-face* TD-OCT provides a lower cost alternative for high transversal resolution of static samples.

We have shown that complementary studies are possible by combining OCT with more traditional methods, such as confocal microscopy and microCT. Combination of principles is expected to evolve in the near future due to their limitations when considered separately.

TD-OCT and SD-OCT systems were used separately in our studies, for different applications, as presented. However, research has shown improved performance achievable by combining principles of TD and SD interferometry. For the moment, implementation of combination of such principles is still expensive, but once implemented, the architectures obtained show promise in terms of simultaneous *en-face* imaging or in terms of extending the axial range of SD methods. They may find niche applications, first in handheld scanning devices and second in long axial catheters to be used on the nerve canals. Dentistry, as well as ophthalmology, will continue to benefit from the continuous advancement in the OCT hardware and customization of different principles to specific applications.

References

1. Fujimoto J.G., Brezinski M.E. Optical coherence tomography imaging. In: *Biomedical photonics handbook.* Vo-Dinh T. (editor). CRC Press; 2003; p. 22–24, http://dx.doi.org/10.1201/9780203008997.ch13.

2. Brady D.J. *Optical imaging and spectroscopy*. Wiley & Sons, Inc.; 2009, http://dx.doi.org/10.1002/9780470443736.

3. *Optical coherence tomography*. Drexler W., Fujimoto J.G. (editors). Springer Berlin Heidelberg; 2008, http://dx.doi.org/10.1007/978-3-540-77550-8.

4. Fercher A.F., Roth E. Ophthalmic laser interferometry. *Proc. SPIE, Optical Instrumentation for Biomedical Laser Applications* 1986; 0658: 48–51, http://dx.doi.org/10.1117/12.938523.

5. Huang D., Swanson E.A., Lin C.P., Schuman J.S., Stinson W.G., Chang W., Hee M.R., Flotte T., Gregory K., Puliafito C.A., Fujimoto J.G. Optical coherence tomography. *Science* 1991; 254(5035): 1178–1181, http://dx.doi.org/10.1126/science.1957169.

6. Podoleanu A.G., Dobre G.M., Webb D.J., Jackson D.A. Coherence imaging by use of a Newton rings sampling function. *Opt Lett* 1996; 21(21): 1789–1791, http://dx.doi.org/10.1364/ol.21.001789.

7. Podoleanu A.G., Dobre G.M., Jackson D.A. En-face coherence imaging using galvanometer scanner modulation. *Opt Lett* 1998; 23(3): 147–149, http://dx.doi.org/10.1364/ol.23.000147.

8. Podoleanu A.G., Seeger M., Dobre G.M., Webb D.J., Jackson D.A., Fitzke F.W. Transversal and longitudinal images from the retina of the living eye using low coherence reflectometry. *J Biomed Opt* 1998; 3(1): 12–20, http://dx.doi.org/10.1117/1.429859.

9. Fercher A.F. Optical coherence tomography — development, principles, applications. *Z Med Phys* 2010; 20(4): 251–276, http://dx.doi.org/10.1016/j.zemedi.2009.11.002.

10. Choma M.A., Sarunic M.V., Yang C., Izatt J.A. Sensitivity advantage of swept source and Fourier domain optical coherence tomography. *Opt Express* 2003; 11(18): 2183–2189, http://dx.doi.org/10.1364/OE.11.002183.

11. Leitgeb R., Hitzenberger C.K., Fercher A.F. Performance of Fourier domain vs. time domain optical coherence tomography. *Opt Express* 2003; 11(8): 889–894, http://dx.doi.org/10.1364/oe.11.000889.

12. Masters B.R. Three-dimensional confocal microscopy of the human optic nerve in vivo. *Opt Express* 1998; 3(10): 356–359, http://dx.doi.org/10.1364/oe.3.000356.

13. Park B.H., Pierce M.C., Cense B., Yun S.-H., Mujat M., Tearney G.J., Bouma B.E., de Boer J.F. Real-time fiber-based multi-functional spectral-domain optical coherence tomography at 1.3 μm. *Opt Express* 2005; 13(11): 3931–44, http://dx.doi.org/10.1364/opex.13.003931.

14. Wang K., Ding Z., Wu T., Wang C., Meng J., Chen M., Xu L. Development of a non-uniform discrete Fourier transform based high speed spectral domain optical coherence

tomography system. *Opt Express* 2009; 17(14): 12121–1231, http://dx.doi.org/10.1364/oe.17.012121.

15. Gützinger E., Baumann B., Pircher M., Hitzenberger C.K. Polarization maintaining fiber based ultra-high resolution spectral domain polarization sensitive optical coherence tomography. *Opt Express* 2009; 17(25): 22704–22717, http://dx.doi.org/10.1364/oe.17.022704.

16. Wang Y., Nelson J.S., Chen Z., Reiser B.J., Chuck R.S., Windeler R.S. Optimal wavelength for ultrahigh-resolution optical coherence tomography. *Opt Express* 2003; 11(12): 1411–1417, http://dx.doi.org/10.1364/OE.11.001411.

17. Bradu A., Ma L., Bloor J.W., Podoleanu A.G. Dual optical coherence tomography/fluorescence microscopy for monitoring of Drosophila melanogaster larval heart. *J Biophotonics* 2009; 2(6–7): 380–388, http://dx.doi.org/10.1002/jbio.200910021.

18. Chen R., Rudney J., Aparicio C., Fok A., Jones R.S. Quantifying dental biofilm growth using cross-polarization optical coherence tomography. *Lett Appl Microbiol* 2012; 54(6): 537–542, http://dx.doi.org/10.1111/j.1472-765X.2012.03243.x.

19. Garcez A.S., Suzuki S.S., Ribeiro M.S., Mada E.Y., Freitas A.Z., Suzuki H. Biofilm retention by 3 methods of ligation on orthodontic brackets: a microbiologic and optical coherence tomography analysis. *Am J Orthod Dentofacial Orthop* 2011; 140(4): e193–e198, http://dx.doi.org/10.1016/j.ajodo.2011.04.019.

20. Mandurah M.M., Sadr A., Bakhsh T.A., Shimada Y., Sumi Y., Tagami J. Characterization of transparent dentin in attrited teeth using optical coherence tomography. *Lasers Med Sci* 2014, [Epub ahead of print], http://dx.doi.org/10.1007/s10103-014-1541-4.

21. Chew H.P., Zakian C.M., Pretty I.A., Ellwood R.P. Measuring initial enamel erosion with quantitative light-induced fluorescence and optical coherence tomography: an in vitro validation study. *Caries Res* 2014; 48(3): 254–262, http://dx.doi.org/10.1159/000354411.

22. Braz A.K., de Araujo R.E., Ohulchanskyy T.Y., Shukla S., Bergey E.J., Gomes A.S.L., Prasad P.N. In situ gold nanoparticles formation: contrast agent for dental optical coherence tomography. *J Biomed Opt* 2012; 17(6): 066003, http://dx.doi.org/10.1117/1.JBO.17.6.066003.

23. Hariri I., Sadr A., Shimada Y., Tagami J., Sumi Y. Effects of structural orientation of enamel and dentine on light attenuation and local refractive index: an optical coherence tomography study. *J Dent* 2012; 40(5): 387–396, http://dx.doi.org/10.1016/j.jdent.2012.01.017.

24. Manesh S.K., Darling C.L., Fried D. Nondestructive assessment of dentin demineralization using polarization-sensitive optical coherence tomography after exposure to fluoride and laser irradiation. *J Biomed Mater Res B Appl Biomater* 2009; 90B(2): 802–812, http://dx.doi.org/10.1002/jbm.b.31349.

25. Manesh S.K., Darling C.L., Fried D. Imaging natural and artificial demineralization on dentin surfaces with polarization sensitive optical coherence tomography. *Proc. SPIE, Lasers in Dentistry XIV* 2008; 6843: 68430M, http://dx.doi.org/10.1117/12.778788.

26. Brady E., Mannocci F., Brown J., Wilson R., Patel S. A comparison of cone beam computed tomography and periapical radiography for the detection of vertical root fractures in nonendodontically treated teeth. *Int Endod J* 2014; 47(8): 735–746, http://dx.doi.org/10.1111/iej.12209.

27. Shemesh H., van Soest G., Wu M.-K., Wesselink P.R. Diagnosis of vertical root fractures with optical coherence tomography. *J Endod* 2008; 34(6): 739–742, http://dx.doi.org/10.1016/j.joen.2008.03.013.

28. Amaechi B.T., Podoleanu A., Higham S.M., Jackson D.A. Correlation of quantitative light-induced fluorescence and optical coherence tomography applied for detection and quantification of early dental caries. *J Biomed Opt* 2003; 8(4): 642–647, http://dx.doi.org/10.1117/1.1606685.

29. Clarkson D.M. An update on optical coherence tomography in dentistry. *Dent Update* 2014; 41(2): 174–176, 179–180.

30. Holtzman J.S., Ballantine J., Fontana M., Wang A., Calantog A., Benavides E., Gonzalez-Cabezas C., Chen Z., Wilder-Smith P. Assessment of early occlusal caries pre- and post-sealant application — an imaging approach. *Lasers Surg Med* 2014; 46(6): 499–507, http://dx.doi.org/10.1002/lsm.22249.

31. Nakajima Y., Shimada Y., Sadr A., Wada I., Miyashin M., Takagi Y., Tagami J., Sumi Y. Detection of occlusal caries in primary teeth using swept source optical coherence tomography. *J Biomed Opt* 2014 Jan; 19(1): 16020, http://dx.doi.org/10.1117/1.JBO.19.1.016020.

32. Chan K.H., Chan A.C., Fried W.A., Simon J.C., Darling C.L., Fried D. Use of 2D images of depth and integrated reflectivity to represent the severity of demineralization in cross-polarization optical coherence tomography. *J Biophotonics* 2013, [Epub ahead of print], http://dx.doi.org/10.1002/jbio.201300137.

33. Gomez J., Zakian C., Salsone S., Pinto S.C.S., Taylor A., Pretty I.A., Ellwood R. In vitro performance of different methods in detecting occlusal caries lesions. *J Dent* 2013; 41(2): 180–186, http://dx.doi.org/10.1016/j.jdent.2012.11.003.

34. Nakagawa H., Sadr A., Shimada Y., Tagami J., Sumi Y. Validation of swept source optical coherence tomography (SS-OCT) for the diagnosis of smooth surface caries in vitro. *J Dent* 2013; 41(1): 80–89, http://dx.doi.org/10.1016/j.jdent.2012.10.007.

35. Nazari A., Sadr A., Campillo-Funollet M., Nakashima S., Shimada Y., Tagami J., Sumi Y. Effect of hydration on assessment of early enamel lesion using swept-source optical coherence tomography. *J Biophotonics* 2013; 6(2): 171–177, http://dx.doi.org/10.1002/jbio.201200012.

36. de Azevedo C.S., Trung L.C.E., Simionato M.R.L., de Freitas A.Z., Matos A.B. Evaluation of caries-affected dentin with optical coherence tomography. *Braz Oral Res* 2011; 25(5): 407–413, http://dx.doi.org/10.1590/S1806-83242011000500006.

37. Chen Y., Otis L., Zhu Q. Polarization memory effect in optical coherence tomography and dental imaging application. *J Biomed Opt* 2011; 16(8): 086005, http://dx.doi.org/10.1117/1.3606573.

38. Kang H., Jiao J.J., Lee C., Le M.H., Darling C.L., Fried D. Nondestructive assessment of early tooth demineralization using cross-polarization optical coherence tomography. *IEEE J Sel Top Quantum Electron* 2010; 16(4): 870–876, http://dx.doi.org/10.1109/JSTQE.2009.2033610.

39. Holtzman J.S., Osann K., Pharar J., Lee K., Ahn Y.C., Tucker T., Sabet S., Chen Z., Gukasyan R., Wilder-Smith P. Ability of optical coherence tomography to detect caries beneath commonly used dental sealants. *Lasers Surg Med* 2010; 42(8): 752–759, http://dx.doi.org/10.1002/lsm.20963.

40. Huminicki A., Dong C., Cleghorn B., Sowa M., Hewko M., Choo-Smith L.P. Determining the effect of calculus, hypocalcification, and stain on using optical coherence

tomography and polarized Raman spectroscopy for detecting white spot lesions. *Int J Dent* 2010; 2010: 879252, http://dx.doi.org/10.1155/2010/879252.

41. Shimada Y., Sadr A., Burrow M.F., Tagami J., Ozawa N., Sumi Y. Validation of swept-source optical coherence tomography (SS-OCT) for the diagnosis of occlusal caries. *J Dent* 2010; 38(8): 655–665, http://dx.doi.org/10.1016/j.jdent.2010.05.004.

42. Maia A.M., Fonsêca D.D., Kyotoku B.B., Gomes A.S. Characterization of enamel in primary teeth by optical coherence tomography for assessment of dental caries. *Int J Paediatr Dent* 2010; 20(2): 158–164, http://dx.doi.org/10.1111/j.1365-263X.2009.01025.x.

43. Tao Y.C., Fried D. Selective removal of natural occlusal caries by coupling near-infrared imaging with a CO_2 laser. *Proc. SPIE, Lasers in Dentistry XIV* 2008; 6843: 68430I, http://dx.doi.org/10.1117/12.778790.

44. Jones R.S., Darling C.L., Featherstone J.D., Fried D. Imaging artificial caries on the occlusal surfaces with polarization-sensitive optical coherence tomography. *Caries Res* 2006; 40(2): 81–89, http://dx.doi.org/10.1159/000091052.

45. Fried D., Xie J., Shafi S., Featherstone J.D.B., Breunig T.M., Le C. Imaging caries lesions and lesion progression with polarization sensitive optical coherence tomography. *J Biomed Opt* 2002; 7(4): 618–627, http://dx.doi.org/10.1117/1.1509752.

46. Amaechi B.T., Higham S.M., Podoleanu A.G., Rogers J.A., Jackson D.A. Use of optical coherence tomography for assessment of dental caries: quantitative procedure. *J Oral Rehabil* 2001; 28(12): 1092–1093, http://dx.doi.org/10.1046/j.1365-2842.2001.00840.x.

47. Colston B.W.Jr., Sathyam U.S., DaSilva L.B., Everett M.J., Stroeve P., Otis L.L. Dental OCT. *Opt Express* 1998; 3(6): 230–238, http://dx.doi.org/10.1364/oe.3.000230.

48. Darling C.L., Staninec M., Chan K.H., Kang H., Fried D. Remineralization of root caries monitored using cross-polarization optical coherence tomography. *Proc. SPIE, Lasers in Dentistry XVIII* 2012; 8208: 82080V, http://dx.doi.org/10.1117/12.914633.

49. Manesh S.K., Darling C.L., Fried D. Polarization-sensitive optical coherence tomography for the nondestructive assessment of the remineralization of dentin. *J Biomed Opt* 2009; 14(4): 044002, http://dx.doi.org/10.1117/1.3158995.

50. Manesh S.K., Darling C.L., Fried D. Assessment of dentin remineralization with PS-OCT. *Proc. SPIE, Lasers in Dentistry XV* 2009; 7162: 71620W, http://dx.doi.org/10.1117/12.816865.

51. Natsume Y., Nakashima S., Sadr A., Shimada Y., Tagami J., Sumi Y. Estimation of lesion progress in artificial root caries by swept source optical coherence tomography in comparison to transverse microradiography. *J Biomed Opt* 2011; 16(7): 071408, http://dx.doi.org/10.1117/1.3600448.

52. Chong S.L., Darling C.L., Fried D. Nondestructive measurement of the inhibition of demineralization on smooth surfaces using polarization-sensitive optical coherence tomography. *Lasers Surg Med* 2007; 39(5): 422–427, http://dx.doi.org/10.1002/lsm.20506.

53. Chong S.L. Detection of white spot lesions around orthodontic brackets using polarization-sensitive optical coherence tomography. *Am J Orthod Dentofacial Orthop* 2007; 132(5): 711, http://dx.doi.org/10.1016/j.ajodo.2007.02.032.

54. Lee R.C., Kang H., Darling C.L., Fried D. Automated assessment of the remineralization of artificial enamel lesions with polarization-sensitive optical coherence tomography. *Biomed Opt Express* 2014; 5(9): 2950–2962, http://dx.doi.org/10.1364/BOE.5.002950.

55. Mandurah M.M., Sadr A., Shimada Y., Kitasako Y., Nakashima S., Bakhsh T.A., Tagami J., Sumi Y. Monitoring remineralization of enamel subsurface lesions by optical coherence tomography. *J Biomed Opt* 2013; 18(4): 046006, http://dx.doi.org/10.1117/1.JBO.18.4.046006.

56. Kang H., Darling C.L., Fried D. Nondestructive monitoring of the repair of enamel artificial lesions by an acidic remineralization model using polarization-sensitive optical coherence tomography. *Dent Mater* 2012; 28(5): 488–494, http://dx.doi.org/10.1016/j.dental.2011.11.020.

57. Jones R.S., Fried D. Remineralization of enamel caries can decrease optical reflectivity. *J Dent Res* 2006; 85(9): 804–808, http://dx.doi.org/10.1177/154405910608500905.

58. Benson P.E., Shah A.A., Willmot D.R. Polarized versus nonpolarized digital images for the measurement of demineralization surrounding orthodontic brackets. *The Angle Orthodontist* 2008; 78(2): 288–293, http://dx.doi.org/10.2319/121306-511.1.

59. Kotaku M., Murayama R., Shimamura Y., Takahashi F., Suzuki T., Kurokawa H., Miyazaki M. Evaluation of the effects of fluoride-releasing varnish on dentin demineralization using optical coherence tomography. *Dent Mater J* 2014; 33(5): 648–655, http://dx.doi.org/10.4012/dmj.2014-072.

60. Arnaud T.M.S., de Barros Neto B., Diniz F.B. Chitosan effect on dental enamel de-remineralization: an in vitro evaluation. *J Dent* 2010; 38(11): 848–852, http://dx.doi.org/10.1016/j.jdent.2010.06.004.

61. Lee C., Darling C.L., Fried D. Polarization-sensitive optical coherence tomographic imaging of artificial demineralization on exposed surfaces of tooth roots. *Dent Mater* 2009; 25(6): 721–728, http://dx.doi.org/10.1016/j.dental.2008.11.014.

62. Hsu D.J., Darling C.L., Lachica M.M., Fried D. Nondestructive assessment of the inhibition of enamel demineralization by CO_2 laser treatment using polarization sensitive optical coherence tomography. *J Biomed Opt* 2008; 13(5): 054027, http://dx.doi.org/10.1117/1.2976113.

63. Can A.M., Darling C.L., Ho C., Fried D. Non-destructive assessment of inhibition of demineralization in dental enamel irradiated by a λ=9.3-microm CO_2 laser at ablative irradiation intensities with PS-OCT. *Lasers Surg Med* 2008; 40(5): 342–349, http://dx.doi.org/10.1002/lsm.20633.

64. Hsu D.J., Darling C.L., Fried D. Imaging laser irradiated enamel surfaces with polarization sensitive optical coherence tomography. *Proc. SPIE, Lasers in Dentistry XIV* 2008; 6843: 8430N, http://dx.doi.org/10.1117/12.778789.

65. Pande P., Shrestha S., Park J., Serafino M.J., Gimenez-Conti I., Brandon J., Cheng Y.S., Applegate B.E., Jo J.A. Automated classification of optical coherence tomography images for the diagnosis of oral malignancy in the hamster cheek pouch. *J Biomed Opt* 2014; 19(8): 086022, http://dx.doi.org/10.1117/1.JBO.19.8.086022.

66. Hamdoon Z., Jerjes W., Upile T., McKenzie G., Jay A., Hopper C. Optical coherence tomography in the assessment of suspicious oral lesions: an immediate ex vivo study. *Photodiagnosis Photodyn Ther* 2013; 10(1): 17–27, http://dx.doi.org/10.1016/j.pdpdt.2012.07.005.

67. Adegun O.K., Tomlins P.H., Hagi-Pavli E., Bader D.L., Fortune F. Quantitative optical coherence tomography of fluid-

filled oral mucosal lesions. *Lasers Med Sci* 2013; 28(5): 1249–1255, http://dx.doi.org/10.1007/s10103-012-1208-y.

68. Park K.J., Schneider H., Haak R. Assessment of interfacial defects at composite restorations by swept source optical coherence tomography. *J Biomed Opt* 2013; 18(7): 076018, http://dx.doi.org/10.1117/1.JBO.18.7.076018.

69. Nazari A., Sadr A., Shimada Y., Tagami J., Sumi Y. 3D assessment of void and gap formation in flowable resin composites using optical coherence tomography. *J Adhes Dent* 2013; 15(3): 237–243, http://dx.doi.org/10.3290/j.jad.a28623.

70. Shimada Y., Nakagawa H., Sadr A., Wada I., Nakajima M., Nikaido T., Otsuki M., Tagami J., Sumi Y. Noninvasive cross-sectional imaging of proximal caries using swept-source optical coherence tomography (SS-OCT) in vivo. *J Biophotonics* 2014; 7(7): 506–513, http://dx.doi.org/10.1002/jbio.201200210.

71. Lammeier C., Li Y., Lunos S., Fok A., Rudney J., Jones R.S. Influence of dental resin material composition on cross-polarization-optical coherence tomography imaging. *J Biomed Opt* 2012; 17(10): 106002, http://dx.doi.org/10.1117/1.JBO.17.10.106002.

72. Nazari A., Sadr A., Saghiri M.A., Campillo-Funollet M., Hamba H., Shimada Y., Tagami J., Sumi Y. Non-destructive characterization of voids in six flowable composites using swept-source optical coherence tomography. *Dent Mater* 2013; 29(3): 278–286, http://dx.doi.org/10.1016/j.dental.2012.11.004.

73. Bakhsh T.A., Sadr A., Shimada Y., Mandurah M.M., Hariri I., Alsayed E.Z., Tagami J., Sumi Y. Concurrent evaluation of composite internal adaptation and bond strength in a class-I cavity. *J Dent* 2013; 41(1): 60–70, http://dx.doi.org/10.1016/j.jdent.2012.10.003.

74. Shimada Y., Sadr A., Nazari A., Nakagawa H., Otsuki M., Tagami J., Sumi Y. 3D evaluation of composite resin restoration at practical training using swept-source optical coherence tomography (SS-OCT). *Dent Mater J* 2012; 31(3): 409–417, http://dx.doi.org/10.4012/dmj.2011-244.

75. Monteiro G.Q.M., Montes M.A.J.R., Gomes A.S.L., Mota C.C.B.O., Campello S.L., Freitas A.Z. Marginal analysis of resin composite restorative systems using optical coherence tomography. *Dent Mater* 2011; 27(12): e213–e23, http://dx.doi.org/10.1016/j.dental.2011.08.400.

76. Senawongse P., Pongprueksa P., Harnirattisai C., Sumi Y., Otsuki M., Shimada Y., Tagami J. Non-destructive assessment of cavity wall adaptation of class V composite restoration using swept-source optical coherence tomography. *Dent Mater J* 2011; 30(4): 517–522, http://dx.doi.org/10.4012/dmj.2011-061.

77. Bakhsh T.A., Sadr A., Shimada Y., Tagami J., Sumi Y. Non-invasive quantification of resin-dentin interfacial gaps using optical coherence tomography: validation against confocal microscopy. *Dent Mater* 2011; 27(9): 915–925, http://dx.doi.org/10.1016/j.dental.2011.05.003.

78. Ishibashi K., Ozawa N., Tagami J., Sumi Y. Swept-source optical coherence tomography as a new tool to evaluate defects of resin-based composite restorations. *J Dent* 2011; 39(8): 543–548, http://dx.doi.org/10.1016/j.jdent.2011.05.005.

79. Makishi P., Shimada Y., Sadr A., Tagami J., Sumi Y. Non-destructive 3D imaging of composite restorations using optical coherence tomography: marginal adaptation of self-etch adhesives. *J Dent* 2011; 39(4): 316–325, http://dx.doi.org/10.1016/j.jdent.2011.01.011.

80. Matheus T.C., Kauffman C.M., Braz A.K., Mota C.C., Gomes A.S. Fracture process characterization of fiber-reinforced dental composites evaluated by optical coherence tomography, SEM and optical microscopy. *Braz Dent J* 2010; 21(5): 420–427, http://dx.doi.org/10.1590/S0103-64402010000500008.

81. de Melo L.S.A., de Araujo R.E., Freitas A.Z., Zezell D., Vieira N.D., Girkin J., Hall A., Carvalho M.T., Gomes A.S.L. Evaluation of enamel dental restoration interface by optical coherence tomography. *J Biomed Opt* 2005; 10(6): 064027, http://dx.doi.org/10.1117/1.2141617.

82. Braz A.K.S., Aguiar C.M., Gomes A.S.L. Evaluation of the integrity of dental sealants by optical coherence tomography. *Dent Mater* 2011; 27(4): e60–e64, http://dx.doi.org/10.1016/j.dental.2010.11.010.

83. Jones R.S., Staninec M., Fried D. Imaging artificial caries under composite sealants and restorations. *J Biomed Opt* 2004; 9(6): 1297–1304, http://dx.doi.org/10.1117/1.1805562.

84. Otis L.L., al-Sadhan R.I., Meiers J., Redford-Badwal D. Identification of occlusal sealants using optical coherence tomography. *J Clin Dent* 2003; 14(1): 7–10.

85. Minamino T., Mine A., Omiya K., Matsumoto M., Nakatani H., Iwashita T., Ohmi M., Awazu K., Yatani H. Nondestructive observation of teeth post core space using optical coherence tomography: a pilot study. *J Biomed Opt* 2014; 19(4): 046004, http://dx.doi.org/10.1117/1.JBO.19.4.046004.

86. Shemesh H., van Soest G., Wu M.-K., van der Sluis L.W.M., Wesselink P.R. The ability of optical coherence tomography to characterize the root canal walls. *J Endod* 2007; 33(11): 1369–1373, http://dx.doi.org/10.1016/j.joen.2007.06.022.

87. Kikuchi K., Akiba N., Sadr A., Sumi Y., Tagami J., Minakuchi S. Evaluation of the marginal fit at implant — abutment interface by optical coherence tomography. *J Biomed Opt* 2014; 19(5): 055002, http://dx.doi.org/10.1117/1.JBO.19.5.055002.

88. Bista B., Sadr A., Nazari A., Shimada Y., Sumi Y., Tagami J. Nondestructive assessment of current one-step self-etch dental adhesives using optical coherence tomography. *J Biomed Opt* 2013; 18(7): 76020, http://dx.doi.org/10.1117/1.JBO.18.7.076020.

89. Drexler W., Fujimoto J.G. *Optical coherence tomography.* Springer Berlin Heidelberg; 2008, http://dx.doi.org/10.1007/978-3-540-77550-8.

90. Xiang X., Sowa M.G., Iacopino A.M., Maev R.G., Hewko M.D., Man A., Liu K.-Z. An update on novel non-invasive approaches for periodontal diagnosis. *J Periodontol* 2010; 81(2): 186–198, http://dx.doi.org/10.1902/jop.2009.090419.

91. Sumi Y., Ozawa N., Nagaosa S., Minakuchi S., Umemura O. Application of optical coherence tomography (OCT) to nondestructive inspection of dentures. *Arch Gerontol Geriatr* 2011; 53(2): 237–241, http://dx.doi.org/10.1016/j.archger.2010.11.022.

92. Lin C.-L., Kuo W.-C., Chang Y.-H., Yu J.-J., Lin Y.-C. Examination of ceramic/enamel interfacial debonding using acoustic emission and optical coherence tomography. *Dent Mater* 2014; 30(8): 910–916, http://dx.doi.org/10.1016/j.dental.2014.05.023.

93. Nakajima Y., Shimada Y., Miyashin M., Takagi Y., Tagami J., Sumi Y. Noninvasive cross-sectional imaging of incomplete crown fractures (cracks) using swept-source optical coherence tomography. *Int Endod J* 2012; 45(10): 933–941, http://dx.doi.org/10.1111/j.1365-2591.2012.02052.x.

94. Turkistani A., Sadr A., Shimada Y., Nikaido T., Sumi Y.,

Tagami J. Sealing performance of resin cements before and after thermal cycling: evaluation by optical coherence tomography. *Dent Mater* 2014; 30(9): 993–1004, http://dx.doi.org/10.1016/j.dental.2014.05.010.

95. Lin C.-L., Kuo W.-C., Yu J.-J., Huang S.-F. Examination of ceramic restorative material interfacial debonding using acoustic emission and optical coherence tomography. *Dent Mater* 2013; 29(4): 382–388, http://dx.doi.org/10.1016/j.dental.2012.12.003.

96. Na J., Lee B.H., Baek J.H., Choi E.S. Optical approach for monitoring the periodontal ligament changes induced by orthodontic forces around maxillary anterior teeth of white rats. *Med Biol Eng Comput* 2008; 46(6): 597–603, http://dx.doi.org/10.1007/s11517-007-0300-0.

97. Baek J.H., Na J., Lee B.H., Choi E.S., Sone W.S. Optical approach to the periodontal ligament under orthodontic tooth movement: a preliminary study with optical coherence tomography. *Am J Orthod Dentofacial Orthop* 2009; 135(2): 252–259, http://dx.doi.org/10.1016/j.ajodo.2007.10.037.

98. Pithon M.M., dos Santos M.J., Andrade C.S.S., Leão Filho J.C., Braz A.K., de Araujo R.E., Tanaka O.M., Fidalgo T.K., dos Santos A.M., Maia L.C. Effectiveness of varnish with CPP–ACP in prevention of caries lesions around orthodontic brackets: an OCT evaluation. *Eur J Orthod* 2014, [Epub ahead of print], http://dx.doi.org/10.1093/ejo/cju031.

99. Koprowski R., Machoy M., Woźniak K., Wróbel Z. Automatic method of analysis of OCT images in the assessment of the tooth enamel surface after orthodontic treatment with fixed braces. *Biomed Eng Online* 2014; 13: 48, http://dx.doi.org/10.1186/1475-925X-13-48.

100. Isfeld D.M., Aparicio C., Jones R.S. Assessing near infrared optical properties of ceramic orthodontic brackets using cross-polarization optical coherence tomography. *J Biomed Mater Res B Appl Biomater* 2014; 102(3): 516–523, http://dx.doi.org/10.1002/jbm.b.33029.

101. Leão Filho J.C.B., Braz A.K.S., de Souza T.R., de Araujo R.E., Pithon M.M., Tanaka O.M. Optical coherence tomography for debonding evaluation: an in-vitro qualitative study. *Am J Orthod Dentofacial Orthop* 2013; 143(1): 61–68, http://dx.doi.org/10.1016/j.ajodo.2012.08.025.

102. Marcauteanu C., Negrutiu M., Sinescu C., Demjan E., Huges M., Bradu A., Dobre G., Podoleanu A.G. Occlusal overload investigations by noninvasive technology: fluorescence microscopy and en-face optical coherence tomography. *Proc. SPIE, Optical Coherence Tomography and Coherence Techniques IV* 2009; 7372: 737227, http://dx.doi.org/10.1117/12.831797.

103. Mărcăuteanu C., Negrutiu M., Sinescu C., Demjan E., Huges M., Bradu A., Dobre G., Podoleanu A.G. Early detection of tooth wear by en-face optical coherence tomography. *Proc. SPIE, Lasers in Dentistry XV* 2009; 7162: 716205, http://dx.doi.org/10.1117/12.809828.

104. Demjan E., Mărcăuțeanu C., Bratu D., Sinescu C., Negruțiu M., Ionita C., Topală F., Hughes M., Bradu A., Dobre G., Podoleanu A.G. Analysis of dental abfractions by optical coherence tomography. *Proc. SPIE, Lasers in Dentistry XVI* 2010; 7549: 754903, http://dx.doi.org/10.1117/12.842819.

105. The Academy of Prosthodontics. *The glossary of prosthodontic terms.* 8th ed. St. Louis; 2005.

106. Smith B.G., Knight J.K. An index for measuring the wear of teeth. *Br Dent J* 1984; 156(12): 435–438, http://dx.doi.org/10.1038/sj.bdj.4805394.

107. Mărcăuțeanu C., Topală F., Negrutiu M.L., Stoica E.T., Sinescu C. 3D finite element analysis of restorative materials used in dental abfractions. *Solid State Phenomena* 2012; 188: 82–86, http://dx.doi.org/10.4028/www.scientific.net/ssp.188.82.

108. Marcauteanu C., Negrutiu M., Sinescu C., Stoica E.T., Ionita C., Topala F., Vasile L., Bradu A., Dobre G., Podoleanu A.G. Early characterization of occlusal overloaded cervical dental hard tissues by en face optical coherence tomography. *Proc. SPIE, Optical Coherence Tomography and Coherence Techniques V* 2011; 8091: 80911X, http://dx.doi.org/10.1117/12.889711.

109. Marcauteanu C., Bradu A., Sinescu C., Topala F.I., Negrutiu M.L., Podoleanu A.G. Quantitative evaluation of dental abfraction and attrition using a swept-source optical coherence tomography system. *J Biomed Opt* 2014; 19(2): 021108, http://dx.doi.org/10.1117/1.JBO.19.2.021108.

110. Stoica E.T., Marcauteanu C., Bradu A., Sinescu C., Topala F.I., Negrutiu M.L., Duma V.F., Podoleanu A.G. Imaging of noncarious cervical lesions by means of a fast swept source optical coherence tomography system. *Proc. SPIE, Fifth International Conference on Lasers in Medicine: Biotechnologies Integrated in Daily Medicine* 2014; 8925: 89250Y, http://dx.doi.org/10.1117/12.2044214.

111. Marcauteanu C., Bradu A., Sinescu C., Topala F.I., Negrutiu M.L., Duma V.F., Podoleanu A.G. The advantages of a swept source optical coherence tomography system in the evaluation of occlusal disorders. *Proc. SPIE, Fifth International Conference on Lasers in Medicine: Biotechnologies Integrated in Daily Medicine* 2014; 8925: 89250W, http://dx.doi.org/10.1117/12.2044198.

112. Kleinetal T., Wieser W., Eigenwillig C.M., Biedermann B.R., Huber R. Megahertz OCT for ultrawide-field retinal imaging with a 1050 nm Fourier domain mode-locked laser. *Opt Express* 2011; 19(4): 3044–3062, http://dx.doi.org/10.1364/OE.19.003044.

113. Wieser W., Biedermann B.R., Klein T., Eigenwillig C.M., Huber R. Multi-megahertz OCT: high quality 3D imaging at 20 million A-scans and 4.5 GVoxels per second. *Opt Express* 2010; 18(14): 14685–14704, http://dx.doi.org/10.1364/OE.18.014685.

114. Enescu M., Sinescu C., Negrutiu M., Negru R., Marsavina L., Topala F., Rominu R., Petrescu E., Bradu A., Dobre G., Rominu M., Podoleanu A. Amalgam and composite resin interface investigation by optical coherence tomography. *Advances in Communications, Computers, Systems, Circuits and Devices* 2010; p. 316–322.

115. Sinescu C., Marsavina L., Negrutiu M.L., Rusu L.C., Ardelean L., Ionita C., Podoleanu A.G., Rominu M., Topala F.I. Confocal microscopy combined with time domain optical coherence tomography and micro computer tomography in interface evaluation of class II direct composite restoration. *Rev Chim* 2011; 62(10): 1039–1041.

116. Negruțiu M.L., Sinescu C., Topala F., Ionita C., Marcauteanu C., Petrescu E.L., Podoleanu A.G. Imagistic evaluation of direct dental restoration: en face OCT versus SEM and microCT. *Proc. SPIE, Optical Coherence Tomography and Coherence Techniques V* 2011; 8091: 80911T, http://dx.doi.org/10.1117/12.890021.

117. Topala F., Sinescu C., Negrutiu M., Bradu A., Rominu M., Podoleanu A.G. 3D reconstructions of resin dental fillings based on en face OCT images. *Advances in Biology, Bioengineering and Environment* 2010; p. 19–22.

118. Rominu M., Sinescu C., Negrutiu M.L., Rominu R.O.,

Silvana Canjau, Carmen Todea, Meda Lavinia Negrutiu, Cosmin Sinescu, ..., Adrian Gh. Podoleanu

Pop D.M., Topala F., Stoia A., Petrescu E., Bradu A., Dobre G., Podoleanu A.G. Adhesive improvement in optical coherence tomography combined with confocal microscopy for class V cavities investigations. *Proc. SPIE, Medical Imaging 2010: Biomedical Applications in Molecular, Structural, and Functional Imaging* 2010; 7626: 76260Y, http://dx.doi.org/10.1117/12.844538.

119. Marcauteanu C., Negrutiu M.L., Ardelean L., Rusu L.C., Podoleanu A. Evaluation of the prognosis of compomer class V restorations through en face optical coherence tomography. *Rev Chim* 2012; 63(5): 545–547.

120. Sinescu C., Negrutiu M.L., Todea C., Balabuc C., Filip L., Rominu R., Bradu A., Hughes M., Podoleanu A.G. Quality assessment of dental treatments using en-face optical coherence tomography. *J Biomed Opt* 2008; 13(5): 054065, http://dx.doi.org/10.1117/1.2992593.

121. He Y., Wang R.K. Dynamic optical clearing effect of tissue impregnated with hyperosmotic agents and studied with optical coherence tomography. *J Biomed Opt* 2004; 9(1): 200–206, http://dx.doi.org/10.1117/1.1629682.

122. Sinescu C., Marsavina L., Negrutiu M.L., Rusu L.C., Ardelean L., Rominu M., Antoniac I., Topala F.I., Podoleanu A.G. New metallic nanoparticles modified adhesive used for time domain optical coherence tomography evaluation of class II direct composite restoration. *Rev Chim* 2012; 63(4): 380–383.

123. Rominu M., Manescu A., Sinescu C., Negrutiu M.L., Topala F., Rominu R.O., Bradu A., Jackson D.A., Giuliani A., Podoleanu A.G. Zirconia enriched dental adhesive: a solution for OCT contrast enhancement. Demonstrative study by synchrotron radiation microtomography. *Dent Mater* 2014; 30(4): 417–423, http://dx.doi.org/10.1016/j.dental.2014.01.004.

124. Todea C., Balabuc C., Sinescu C., Filip L., Kerezsi C., Calniceanu M., Negrutiu M., Bradu A., Hughes M., Podoleanu A.G. En face optical coherence tomography investigation of apical microleakage after laser-assisted endodontic treatment. *Lasers Med Sci* 2010; 25(5): 629–639, http://dx.doi.org/10.1007/s10103-009-0680-5.

125. Todea C., Podoleanu A.G., Sinescu C., Balabuc C., Filip L., Negrutiu M. OCT investigation of apical microleakage — a preliminary in vitro study. *Lasers Surg Med* 2008; Suppl 20: 15.

126. Negrutiu M.L., Sinescu C., Hughes M., Bradu A., Todea C., Balabuc C.I., Filip L.M., Podoleanu A.G. Root canal filling evaluation using optical coherence tomography. *Proc. SPIE, Biophotonics: Photonic Solutions for Better Health Care* 2008; 6991: 69911T, http://dx.doi.org/10.1117/12.780901.

127. Negrutiu M.L., Nica L., Sinescu C., Topala F., Ionita C., Bradu A., Petrescu E.L., Pop D.M., Rominu M., Podoleanu A.G. SEM and microCT validation for en face OCT imagistic evaluation of endodontically treated human teeth. *Proc. SPIE, Medical Imaging 2011: Physics of Medical Imaging* 2011; 7961: 79614W, http://dx.doi.org/10.1117/12.878320.

128. Negrutiu M.L., Sinescu C., Topala F., Nica L., Ionita C., Marcauteanu C., Goguta L., Bradu A., Dobre G., Rominu M., Podoleanu A.G. Root canal filling evaluation using optical coherence tomography. *Proc. SPIE, Biophotonics: Photonic Solutions for Better Health Care II* 2010; 7715: 77151T, http://dx.doi.org/10.1117/12.854842.

129. Todea C., Balabuc C., Filip L., Calniceanu M., Bradu A., Highes M., Podoleanu A.G. Investigation of Er: YAG laser root canal irradiation using en-face OCT. *Proc.*

SPIE, Optical Coherence Tomography and Coherence Techniques IV 2009; 7372: 7372_1C, http://dx.doi.org/10.1364/ECBO.2009.7372_1C.

130. Negrutiu M., Sinescu C., Topala F., Rominu M., Markovic D., Pop D., Hughes M., Bradu A., Dobre G., Podoleanu A.G. En face optical coherence tomography investigation of interface fiber posts/adhesive cement/root canal wall. *Proc. SPIE, Optical Coherence Tomography and Coherence Techniques IV* 2009; 7372: 7372_1A, http://dx.doi.org/10.1364/ECBO.2009.7372_1A.

131. Mărcăuteanu C., Demjan E., Sinescu C., Negrutiu M., Motoc A., Lighezan R., Vasile L., Hughes M., Bradu A., Dobre G., Podoleanu A.G. Preliminary optical coherence tomography investigation of the temporo-mandibular joint disc. *Proc. SPIE, Optical Coherence Tomography and Coherence Domain Optical Methods in Biomedicine XIV* 2010; 7554: 75542G, http://dx.doi.org/10.1117/12.842783.

132. Sinescu C., Negrutiu M.L., Huges M., Bradu A., Todea C., Rominu R., Dodenciu D., Laissue P.L., Podoleanu A.G. Investigation of bracket bonding for orthodontic treatments using en-face optical coherence tomography. *Proc. SPIE, Biophotonics: Photonic Solutions for Better Health Care* 2008; 6991: 69911M, http://dx.doi.org/10.1117/12.780701.

133. Rominu R.O., Popa M., Sinescu C., Negrutiu M.L., Pop D.M., Rusu L.C., Rominu M., Topala F., Podoleanu A.G. The use of spectral domain optical coherence tomography in orthodontics. *Materiale Plastice* 2012; 49(2): 99–100.

134. Rominu R., Sinescu C., Rominu M., Negrutiu M., Petrescu E., Pop D., Podoleanu A.G. The assessment of orthodontic bonding defects: optical coherence tomography followed by three-dimensional reconstruction. *Proc. SPIE, Optical Complex Systems: OCS11* 2011; 8172: 817214, http://dx.doi.org/10.1117/12.896772.

135. Romînu R.O., Sinescu C., Romînu M., Negrutiu M., Laissue P., Mihali S., Cuc L., Hughes M., Bradu A., Podoleanu A. An innovative approach for investigating the ceramic bracket-enamel interface — optical coherence tomography and confocal microscopy. *Proc. SPIE, 1st Canterbury Workshop on Optical Coherence Tomography and Adaptive Optics* 2008; 7139: 71390O, http://dx.doi.org/10.1117/12.814894.

136. Rominu R.O., Sinescu C., Pop D.M., Hughes M., Bradu A., Rominu M., Podoleanu A.G. En-face optical coherence tomography and fluorescence in evaluation of orthodontic interfaces. *World Academy of Science, Engineering and Technology* 2009; 3: 591–594.

137. Demian D., Duma V.-F., Sinescu C., Negrutiu M.L., Cernat R., Topala F.I., Hutiu G., Bradu A., Podoleanu A.G. Design and testing of prototype handheld scanning probes for optical coherence tomography. *Proc Inst Mech Eng H* 2014; 228(8):743–753, http://dx.doi.org/10.1177/0954411914543963.

138. Sinescu C., Negrutiu M., Tatar R., Terteleac A., Negru R., Hluscu M., Culea L., Rominu M., Marsavina L., Hughes M., Bradu A., Dobre G.M., Marcauteanu C., Demjan E., Podoleanu A.G. Investigation of osteoconductive bone substitute by particles analysis, numerical simulation and optical coherence tomography. *Proc. SPIE, Lasers In Dentistry XV* 2009; 7162: 716207.

139. Negruţiu M.L., Sinescu C., Canjau S., Manescu A., Topală F.I., Hoinoiu B., Romonu M., Mărcăuţeanu C., Duma V., Bradu A., Podoleanu A.G. Bone regeneration assessment by optical coherence tomography and MicroCT synchrotron radiation. *Proc. SPIE, Optical Coherence Tomography and*

Coherence Techniques VI 2013; 8802: 880204, http://dx.doi.org/10.1117/12.2032624.

140. Rusu L.C., Negrutiu M.L., Sinescu C., Hoinoiu B., Topala F.I., Duma V.F., Rominu M., Podoleanu A.G. Time domain optical coherence tomography investigation of bone matrix interface in rat femurs. *Proc. SPIE, International Symposium on Photoelectronic Detection and Imaging 2013: Fiber Optic Sensors and Optical Coherence Tomography* 2013; 8914: 89141H, http://dx.doi.org/10.1117/12.2036345.

141. Sinescu C., Huges M., Bradu A., Negrutiu M., Todea C., Antonie S., Laissue P.L., Rominu M., Podoleanu A.G. Implant bone interface investigated with a non-invasive method: optical coherence tomography. *Proc. SPIE, Biophotonics: Photonic Solutions for Better Health Care* 2008; 6991: 69911L, http://dx.doi.org/10.1117/12.780697.

142. Antonie S., Sinescu C., Negrutiu M., Sticlaru C., Negru R., Laissue F.L., Rominu M., Podoleanu A.G. Investigation of implant bone interface with non-invasive methods: numerical simulation, strain gauges and optical coherence tomography. *Key Engineering Materials* 2008; 399: 193–198, http://dx.doi.org/10.4028/www.scientific.net/KEM.399.193.

143. Negrutiu M.L., Sinescu C., Todea C., Podoleanu A.G. Complete denture analyzed by optical coherence tomography. *Proc. SPIE, Lasers in Dentistry XIV* 2008; 6843: 68430R, http://dx.doi.org/10.1117/12.767106.

144. Sinescu C., Negrutiu M., Todea C., Hughes M., Tudorache F., Podoleanu A.G. Fixed partial denture investigated by optical coherence tomography. *Proc. SPIE, Coherence Domain Optical Methods and Optical Coherence Tomography in Biomedicine XII* 2008; 6847: 684707, http://dx.doi.org/10.1117/12.766315.

145. Fabricky M., Todea C., Sinescu C., Negrutiu M.L., Ardelean L., Rusu L.C., Petrescu E.L., Bratu C., Topala F.I., Podoleanu A.G., Bratu E.A. Integral ceramic inlay evaluation by time domain optical coherence tomography. *Rev Chim* 2012; 63(6): 633–335.

146. Sinescu C., Negrutiu M.L., Rominu R.O., Rusu L.C., Topala F.I., Rominu M., Ardelean L., Podoleanu A. Time domain optical coherence tomography evaluation of polymeric fixed partial prostheses. *Materiale Plastice* 2012; 49(1): 58–61.

147. Sinescu C., Negrutiu M., Topala F., Ionita C., Negru R., Fabriky M., Marcauteanu C., Bradu A., Dobre G., Marsavina L., Rominu M., Podoleanu A. Ceramic and polymeric dental onlays evaluated by photo elasticity, optical coherence tomography and micro computed tomography. *Proc. SPIE, Optical Complex Systems: OCS11* 2011; 8172: 817208, http://dx.doi.org/10.1117/12.896717.

148. Negrutiu M.L., Sinescu C., Draganescu G., Rominu R.O., Rominu M., Rusu L.C., Ardelean L., Pop D.M., Petrescu E.L., Podoleanu A.G., Topala F.I. Laser microspectral analysis for validation of en-face OCT imagistic evaluation of microleakage between the metallic framework and veneer materials in fixed partial prostheses. *Rev Chim* 2011; 62(10): 1185–1188.

149. Petrescu E., Sinescu C., Negrutiu M.L., Rominu R., Pop D.M., Rominu M. Non-invasive imagistic investigation of metal-ceramic crowns. *Proc. SPIE, Optical Sensors and Biophotonics II* 2011; 7990: 79900Y, http://dx.doi.org/10.1117/12.891278.

150. Petrescu E., Sinescu C., Negrutiu M.L., Pop D., Rominu R., Enescu M., Rominu M., Bradu A., Dobre G., Podoleanu A.G. OCT and RX validation of metal-ceramic crowns repaired with ceramic material. *Proc. SPIE, Optical Complex Systems: OCS11* 2011; 8172: 817213, http://dx.doi.org/10.1117/12.896770.

151. Negrutiu M.L., Sinescu C., Topala F.I., Ionita C., Goguta L., Marcauteanu C., Rominu M., Podoleanu A.G. Optical investigations of various polymeric materials used in dental technology. *Proc. SPIE, Optical Complex Systems: OCS11* 2011; 8172: 817216, http://dx.doi.org/10.1117/12.896932.

152. Sinescu C., Negrutiu M.L., Ionita C., Topala F., Petrescu E., Rominu R., Pop D.M., Marsavina L., Negru R., Bradu A., Rominu M., Podoleanu A.G. Radiographic, microcomputer tomography, and optical coherence tomography investigations of ceramic interfaces. *Proc. SPIE, Optical Sensors and Biophotonics II* 2011; 7990: 79900W, http://dx.doi.org/10.1117/12.890272.

153. Sinescu C., Negrutiu M.L., Ionita C., Marsavina L., Negru R., Caplescu C., Bradu A., Topala F., Rominu R.O., Petrescu E., Leretter M., Rominu M., Podoleanu A.G. Morphological characterization of dental prostheses interfaces using optical coherence tomography. *Proc. SPIE, Medical Imaging 2010: Biomedical Applications in Molecular, Structural, and Functional Imaging* 2010; 7626: 76261P, http://dx.doi.org/10.1117/12.844533.

154. Rominu M., Sinescu C., Negrutiu M., Birtea N.M., Petrescu E., Rominu R., Hughes M., Bradu A., Dobre G., Podoleanu A.G. A qualitative approach on marginal adaptation of conditioned dental infrastructures using optical coherence tomography. *Proceedings of the 1st International Conference on Manufacturing Engineering, Quality and Production Systems (Vol. I)*. 2009, p. 255–259.

155. Sinescu C., Negrutiu M., Birtea N.M., Petrescu E., Rominu R.O., Marcautean C., Demjan E., Cuc L., Hughes M., Bradu A., Dobre G., Rominu M., Podoleanu A.G. Time domain and spectral optical coherence tomography investigations of integral ceramic fixed partial dentures. *Proceedings of the 2nd International Conference on Maritime and Naval Science and Engineering*. 2009, p. 77–81.

156. Sinescu C., Negrutiu M., Hughes M., Bradu A., Todea C., Rominu M., Laissue P.L., Podoleanu A.G. An optical coherence tomography investigation of material defects in ceramic fixed partial dental prostheses. *Proc. SPIE, Biophotonics: Photonic Solutions for Better Health Care* 2008; 6991: 69910O, http://dx.doi.org/10.1117/12.780694.

157. Negrutiu M.L., Sinescu C., Hughes M., Bradu A., Goguta L., Rominu M., Negru R., Podoleanu A.G. Fibres reinforced dentures investigated with en-face optical coherence tomography. *Proc. SPIE, Biophotonics: Photonic Solutions for Better Health Care* 2008; 6991: 69911U, http://dx.doi.org/10.1117/12.780904.

158. Negrutiu M.L., Sinescu C., Hughes M., Bradu A., Rominu M., Todea C., Dobre G., Podoleanu A.G. Optical coherence tomography and confocal microscopy investigations of dental prostheses. *Proc. SPIE, 1st Canterbury Workshop on Optical Coherence Tomography and Adaptive Optics* 2008; 7139: 71390N, http://dx.doi.org/10.1117/12.816672.

159. Sinescu C, Negruţiu M.L., Petrescu E., Rominu M., Marcauteanu C., Rominu R., Hughes M., Bradu A., Dobre G., Podoleanu A.G. Marginal adaptation of ceramic veneers investigated with en face optical coherence tomography. *Proc. SPIE, Optical Coherence Tomography and Coherence Techniques IV* 2009; 7372: 73722C, http://dx.doi.org/10.1117/12.831830.

160. Duma V.-F., Lee K.-S., Meemon P., Rolland J.P.

Silvana Canjau, Carmen Todea, Meda Lavinia Negrutiu, Cosmin Sinescu, ..., Adrian Gh. Podoleanu

Experimental investigations of the scanning functions of galvanometer-based scanners with applications in OCT. *Appl Opt* 2011; 50(29): 5735–5749, http://dx.doi.org/10.1364/AO.50.005735.

161. Duma V.-F. Optimal scanning function of a galvanometer scanner for an increased duty cycle. *Opt Eng* 2010; 49(10): 103001, http://dx.doi.org/10.1117/1.3497570.

162. Lu C.D., Kraus M.F., Potsaid B., Choi W., Jayaraman V., Cable A.E., Hornegger J., Duker J.S., Fujimoto J.G. Handheld ultrahigh speed swept source optical coherence tomography instrument using a MEMS scanning mirror. *Biomed Opt Express* 2014; 5(1): 293–311, http://dx.doi.org/10.1364/BOE.5.000293.

163. Jung W., Kim J., Jeon M., Chaney E.J, Stewart C.N., Boppart S.A. Handheld optical coherence tomography scanner for primary care diagnostics. *IEEE Trans Biomed Eng* 2011; 58(3): 741–744, http://dx.doi.org/10.1109/TBME.2010.2096816.

164. Cernat R., Tatla T.S., Pang J., Tadrous P.J., Bradu A., Dobre G., Gelikonov G., Gelikonov V., Podoleanu A.G. Dual instrument for in vivo and ex vivo *OCT* imaging in an ENT department. *Biomed Opt Express* 2012; 3: 346–3356, http://dx.doi.org/10.1364/BOE.3.003346.